Supporting Information

Structures, Spectroscopic Properties, and Dioxygen reactivity of 5- and 6-coordinate Nonheme Iron(II) Complexes: A Combined Enzyme/Model Study of Thiol Dioxygenases

Jesse B. Gordon[†], Jeremy P. McGale[†], Joshua R. Prendergast[‡], Zahra Shirani-Sarmazeh[‡], Maxime A. Siegler[†], Guy N. L. Jameson[‡]*, David P. Goldberg[†]*

†Department of Chemistry, The Johns Hopkins University, 3400 North Charles Street, Baltimore, Maryland, 21218, USA

‡ School of Chemistry, Bio21 Molecular Science and Biotechnology Institute, The University of Melbourne, 30 Flemington Road, Parkville, Victoria 3010, Australia

Table of Contents

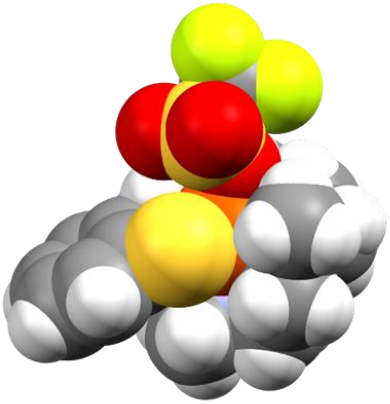

$Fe^{II}(Me_3TACN)(abt)(OTf)$ (**1**)

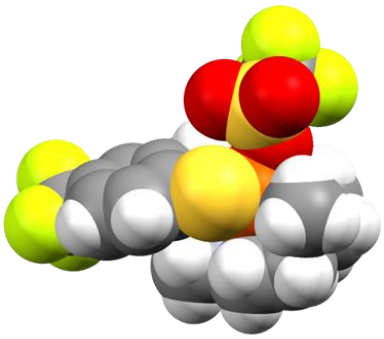

$Fe^{II}(Me_3TACN)(abt^{CF3})(OTf)$ (**2**)

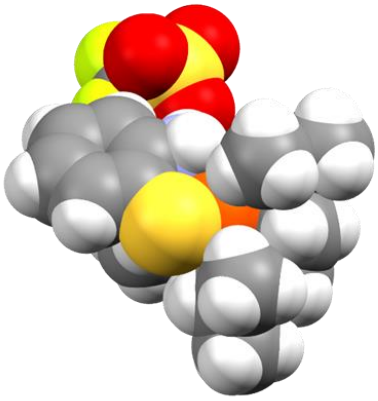

$[Fe^{II}(iPr_3TACN)(abt)](OTf)$ (**3**)

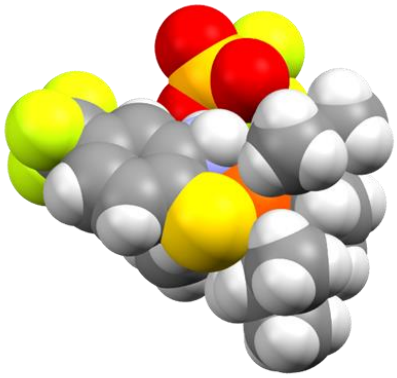

$[Fe^{II}(iPr_3TACN)(abt^{CF3})](OTf)$ (**4**)

Figure S1. Space-filling model for the molecular structures of **1** – **4** at 110(2) K. Fe, S, F, O, N, C, and H atoms shown in orange, yellow, lime green, red, blue, grey, and white respectively.

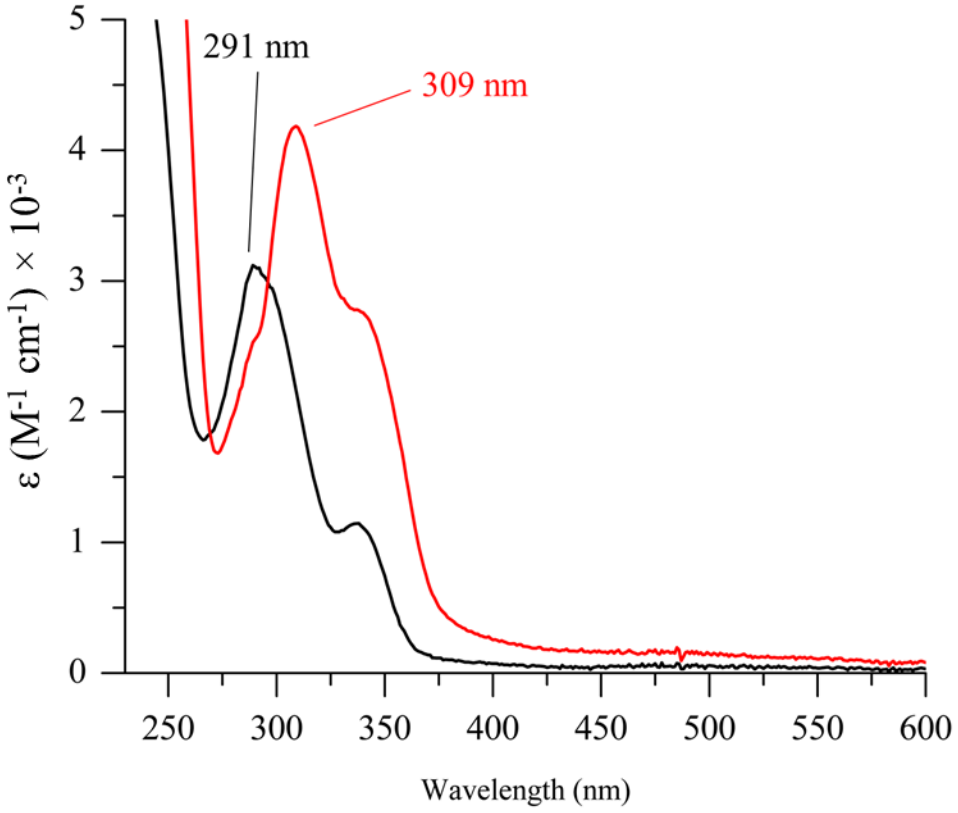

Figure S2. Electronic absorption spectra of 2-aminothiophenol (black line) and 2-amino-4-(trifluoromethyl)benzenethiol (red line) in CH_3CN at 23 °C.

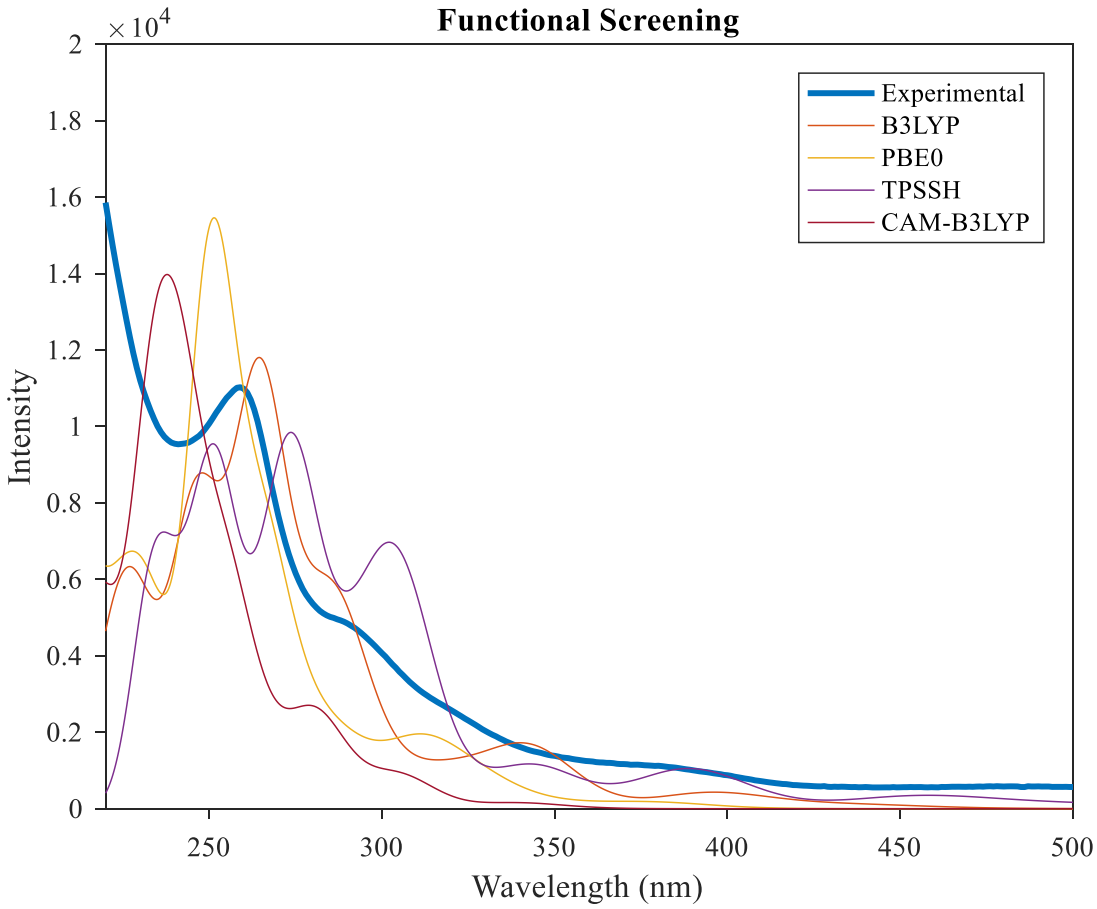

Figure S3. TD-DFT computed absorption spectra for **3** using different functionals.

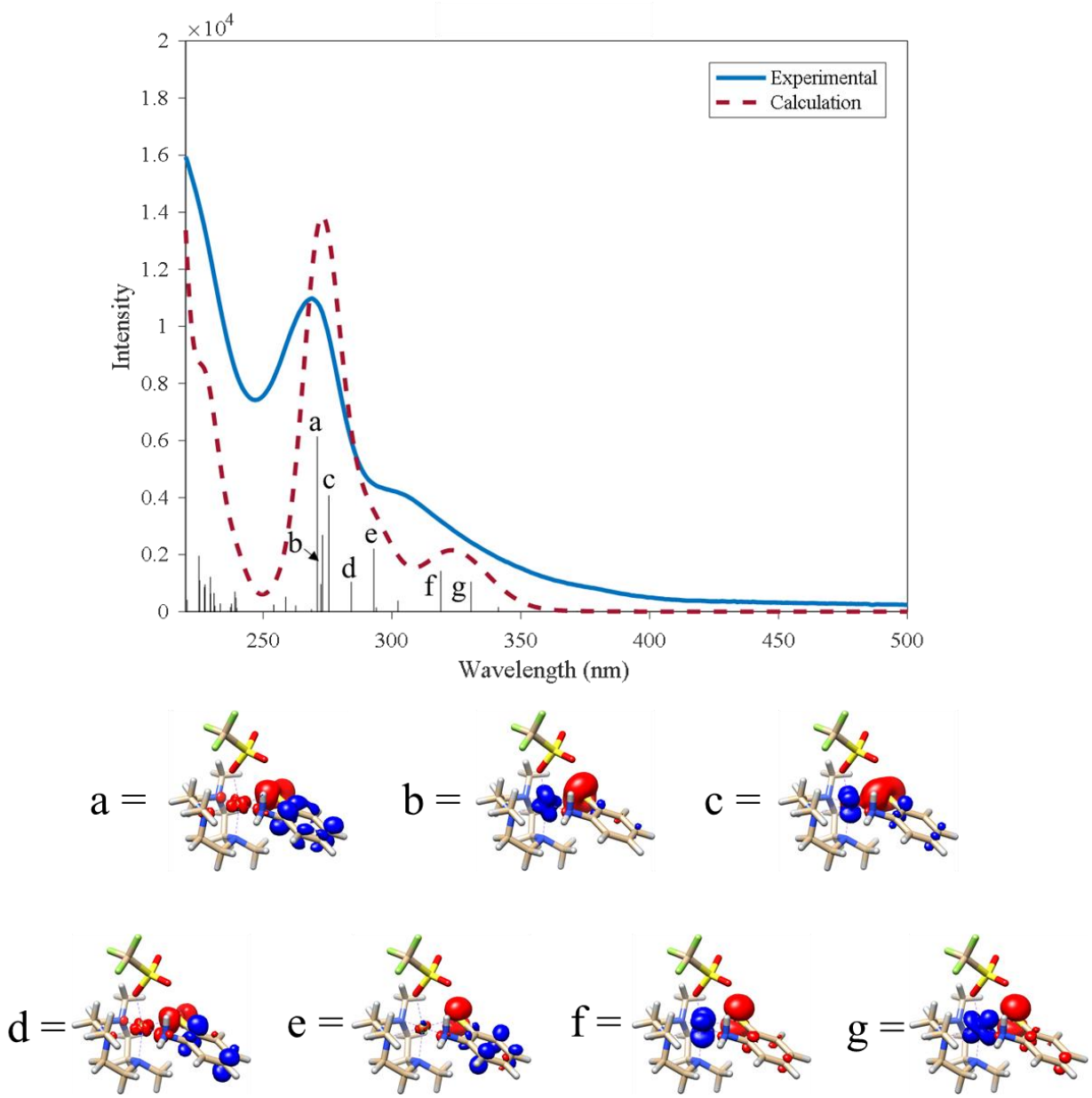

Figure S4. TD-DFT computed absorption spectra for **1** (red dashed line) overlaid with experimental spectra (blue line). The black sticks and letters mark the energies and intensities of calculated transitions. Electron difference density maps for each labeled computed transition is shown below. The blue and red regions indicating gain and loss of electron density, respectively.

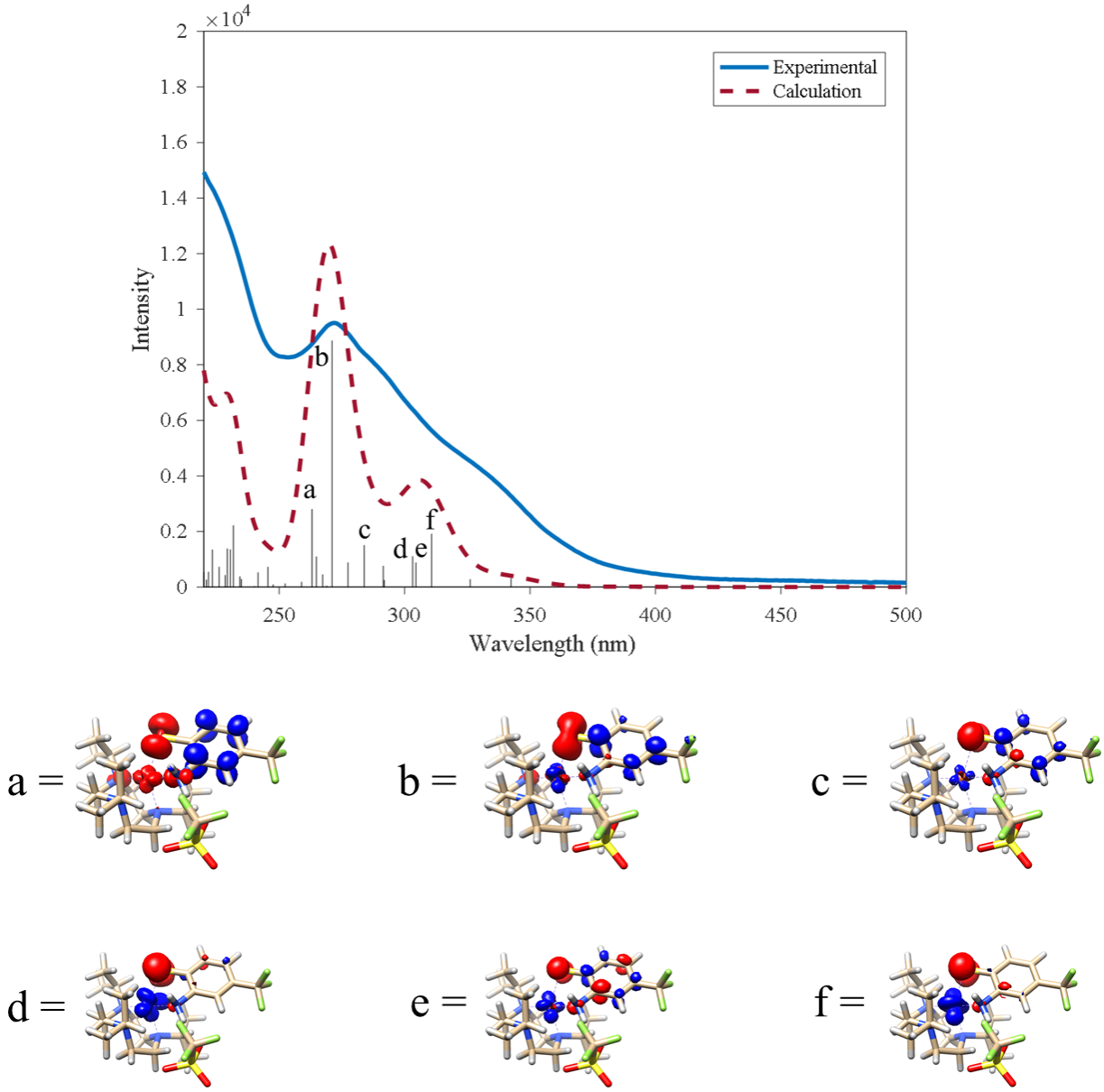

Figure S5. TD-DFT computed absorption spectra for **2** (red dashed line) overlaid with experimental spectra (blue line). The black sticks and letters mark the energies and intensities of calculated transitions. Electron difference density maps for each labeled computed transition is shown below. The blue and red regions indicating gain and loss of electron density, respectively.

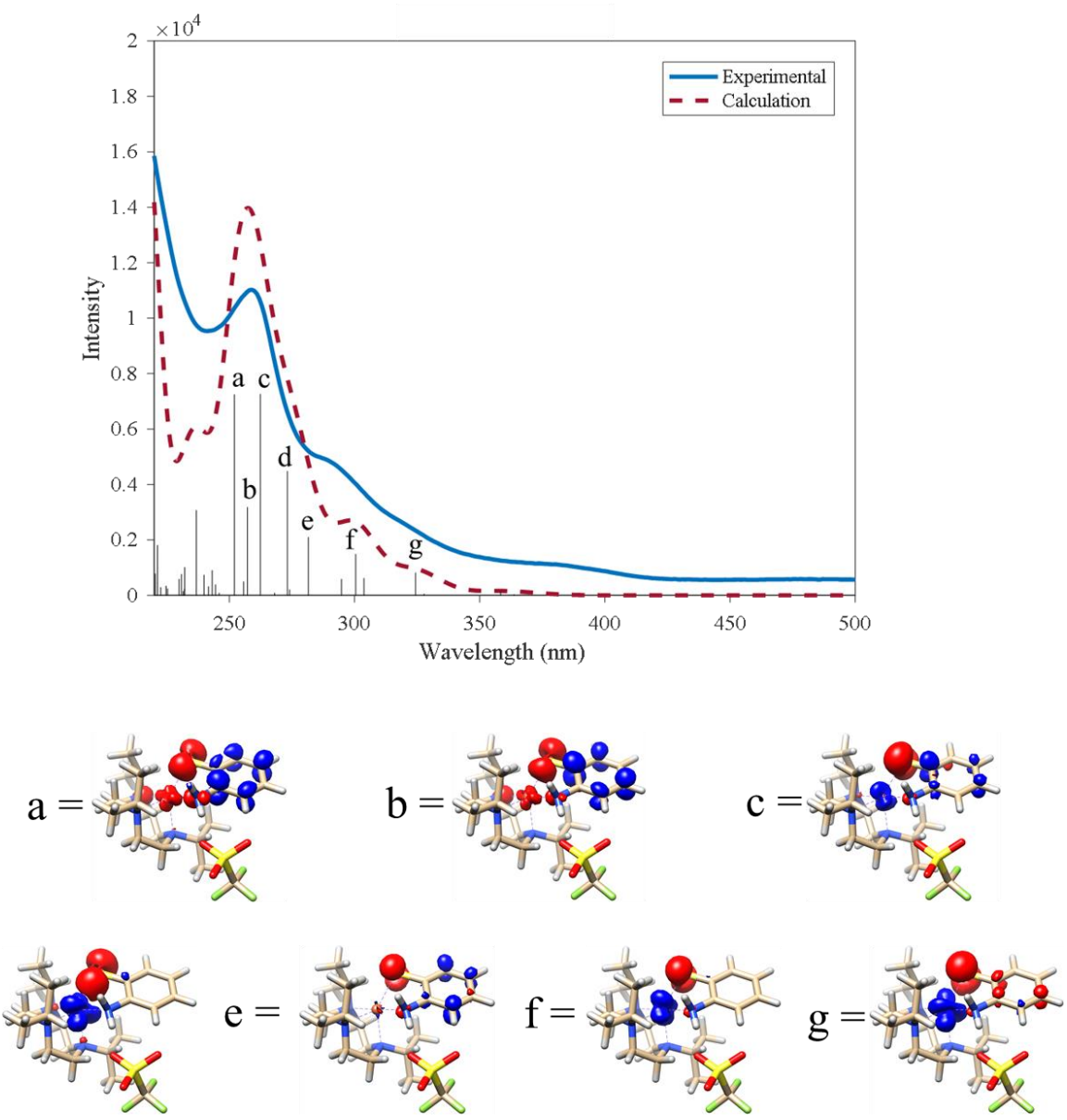

Figure S6. TD-DFT computed absorption spectra for **3** (red dashed line) overlaid with experimental spectra (blue line). The black sticks and letters mark the energies and intensities of calculated transitions. Electron difference density maps for each labeled computed transition is shown below. The blue and red regions indicating gain and loss of electron density, respectively.

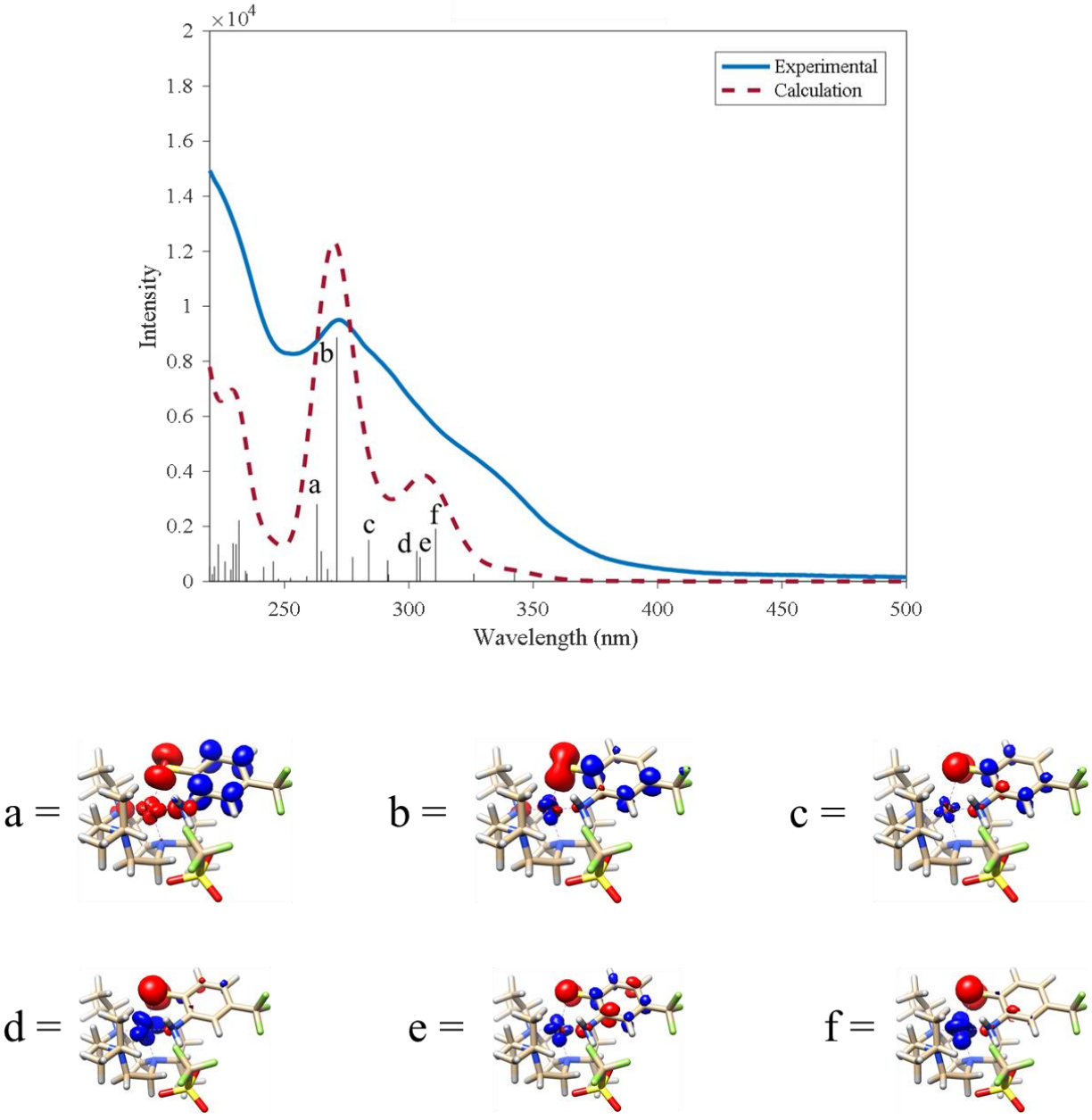

Figure S7. TD-DFT computed absorption spectra for **4** (red dashed line) overlaid with experimental spectra (blue line). The black sticks and letters mark the energies and intensities of calculated transitions. Electron difference density maps for each labeled computed transition is shown below. The blue and red regions indicating gain and loss of electron density, respectively.

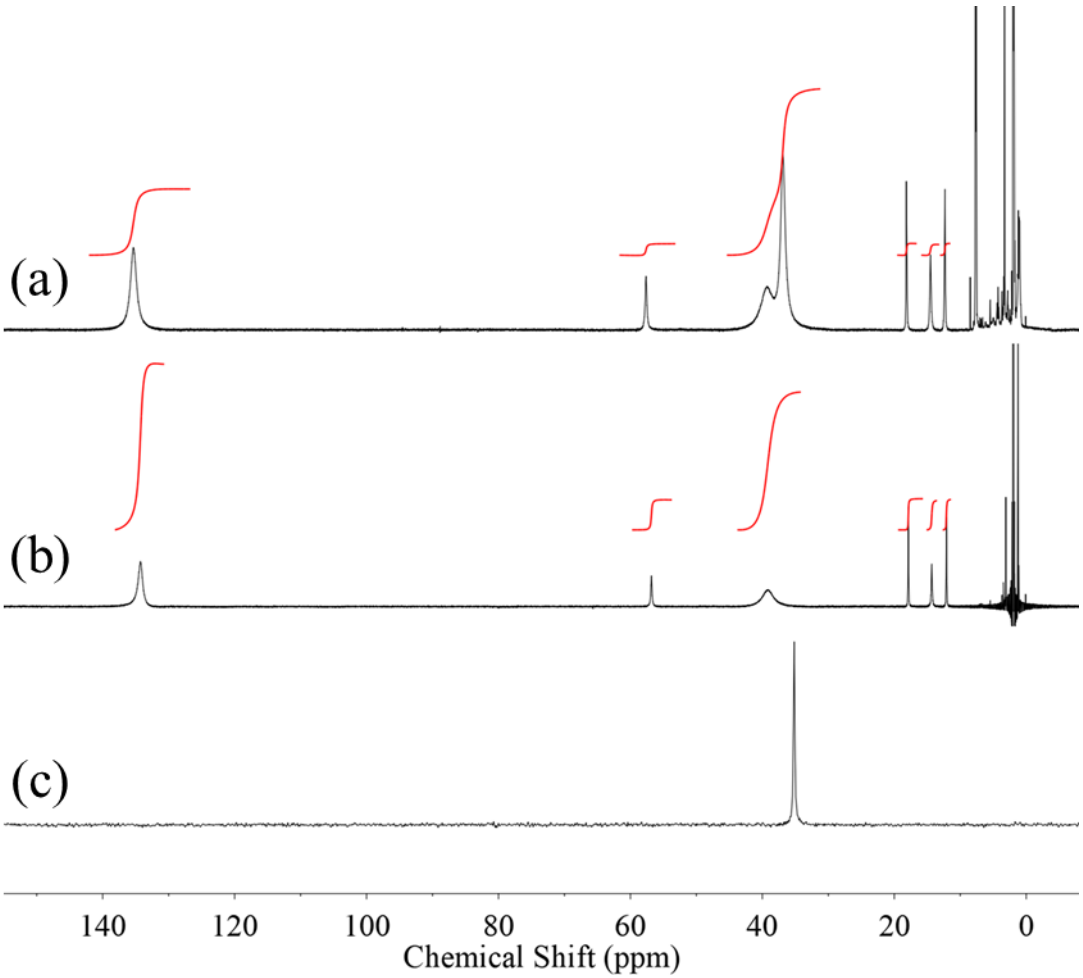

Figure S8. ^{1}H NMR spectra of (a) **1** and (b) $Fe^{II}((CD_3)_3TACN)(abt)(OTf)$ (**1-*d*$_9$**) at 24 °C in CD_3CN and (c) ^{2}H NMR spectrum of **1-*d*$_9$** in acetonitrile at 24 °C.

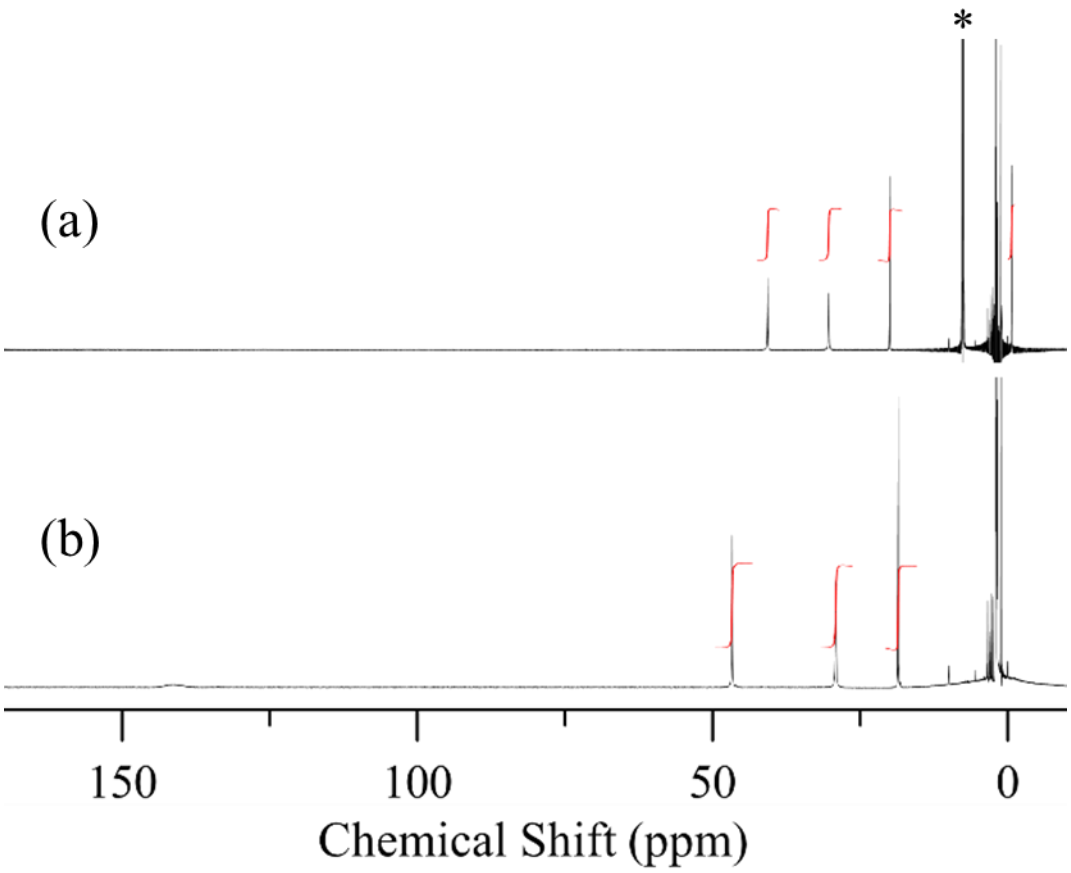

Figure S9. ^{1}H NMR spectra of (a) **3** and (b) **4** in CD_3CN at 24 °C. 1,1,1-trifluorotoluene internal standard designated with an asterisk (*).

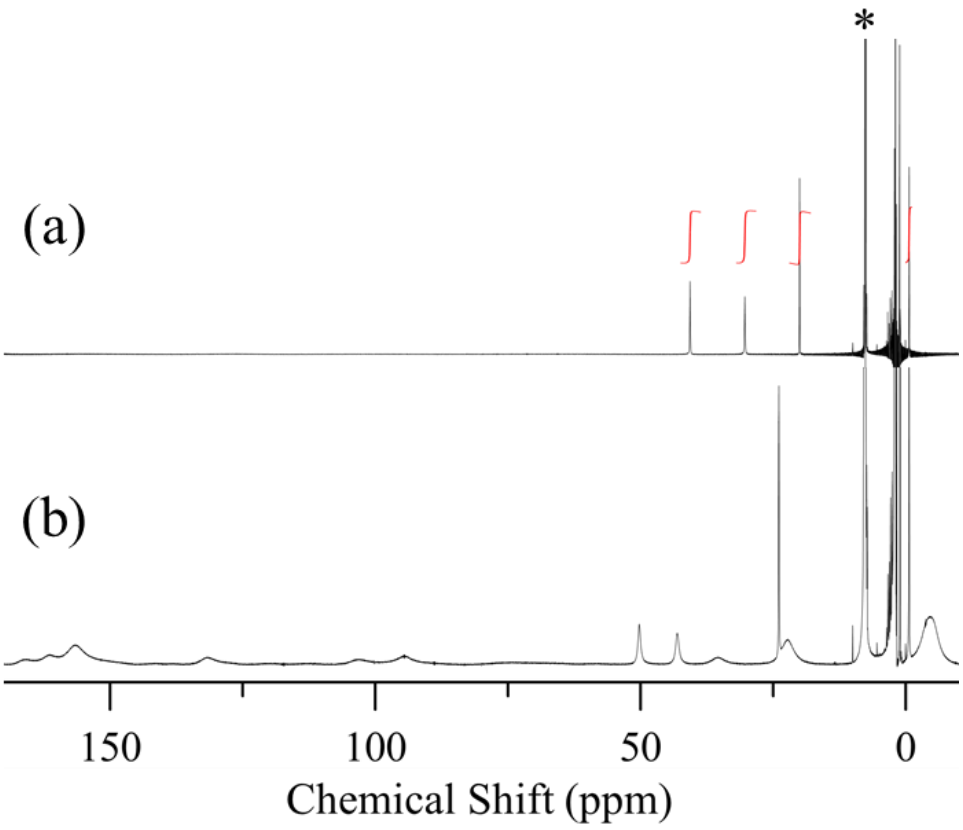

Figure S10. Variable temperature ^{1}H NMR spectra of **3** in CD_3CN at (a) 24 °C and (b) -40 °C. 1,1,1-trifluorotoluene internal standard designated with an asterisk (*).

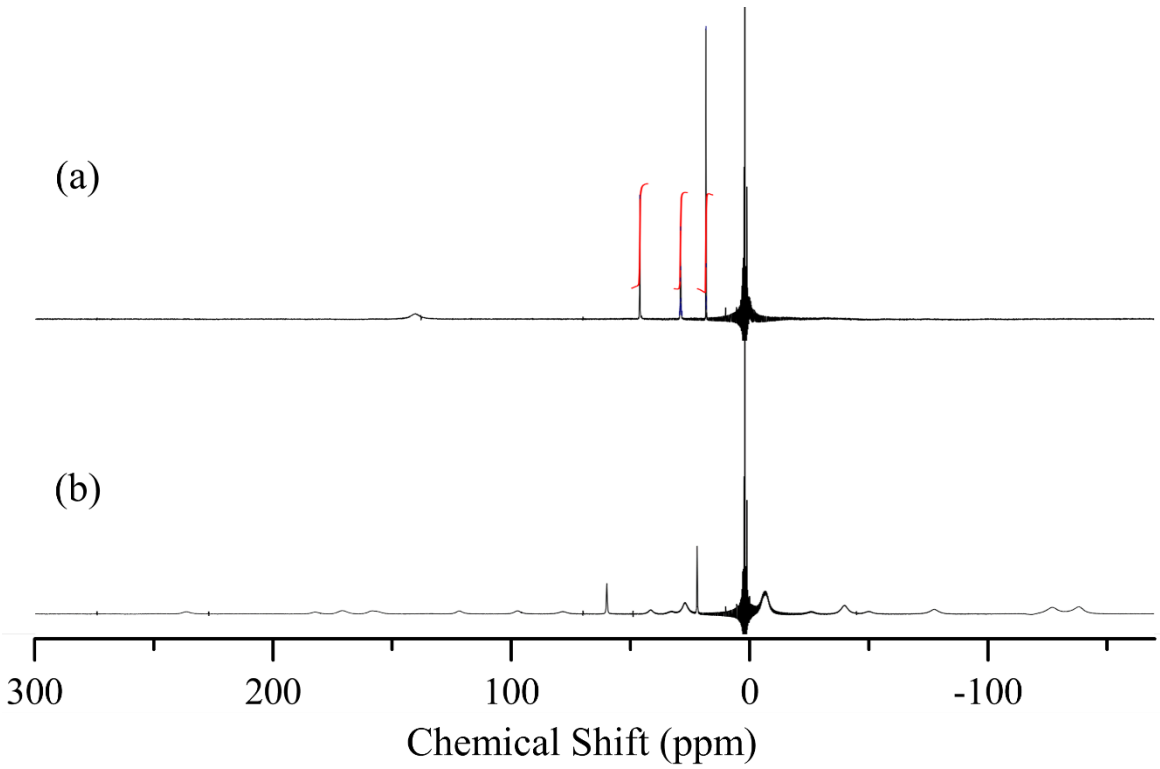

Figure S11. Variable temperature ^{1}H NMR spectra of **4** in CD_3CN at (a) 24 °C and (b) -40 °C.

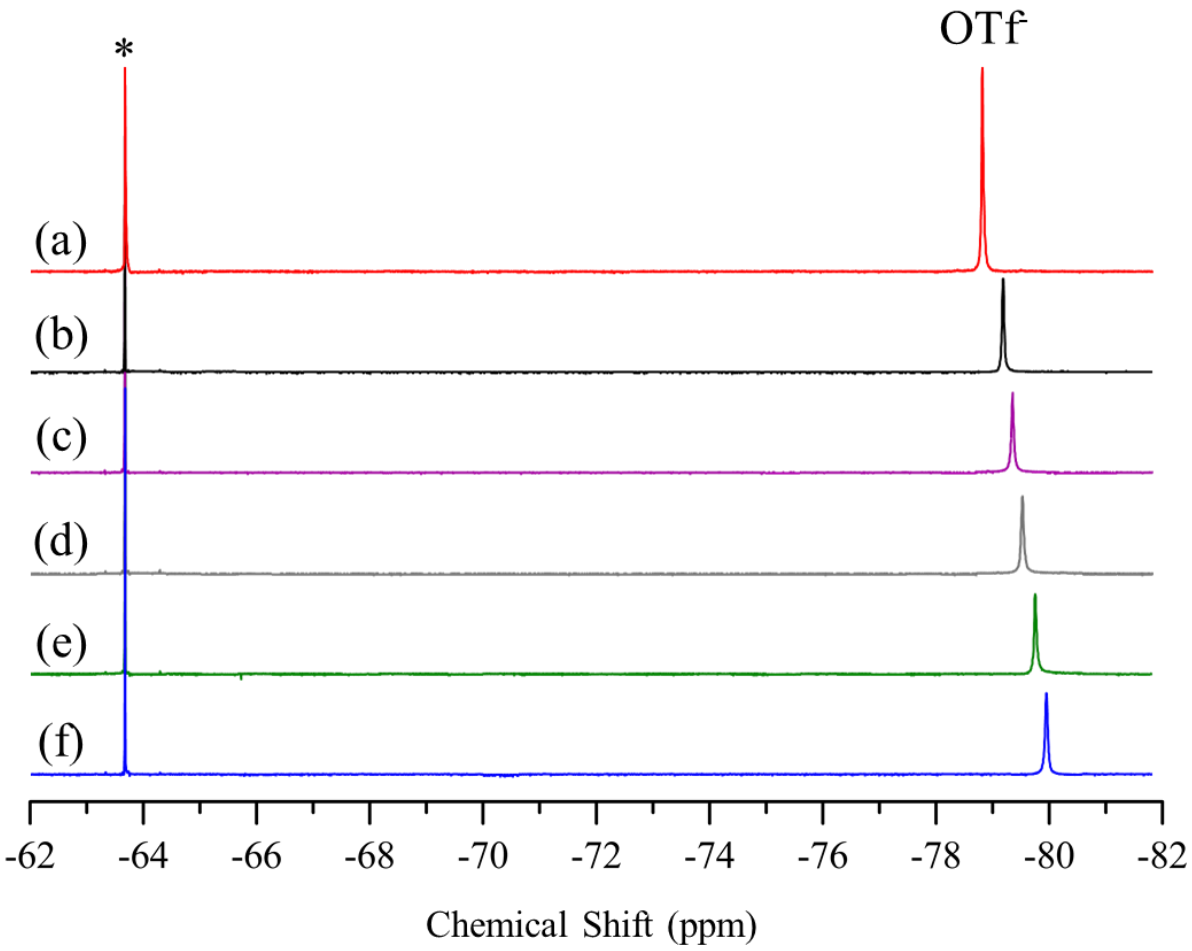

Figure S12. Variable temperature ^{19}F NMR spectra of **1** in CD_3CN at (a) 24 °C, (b) 0 °C, (c) -10 °C, (d) -20 °C, (e) -30 °C, and (f) -40 °C. 1,1,1-trifluorotoluene internal standard designated with an asterisk (*).

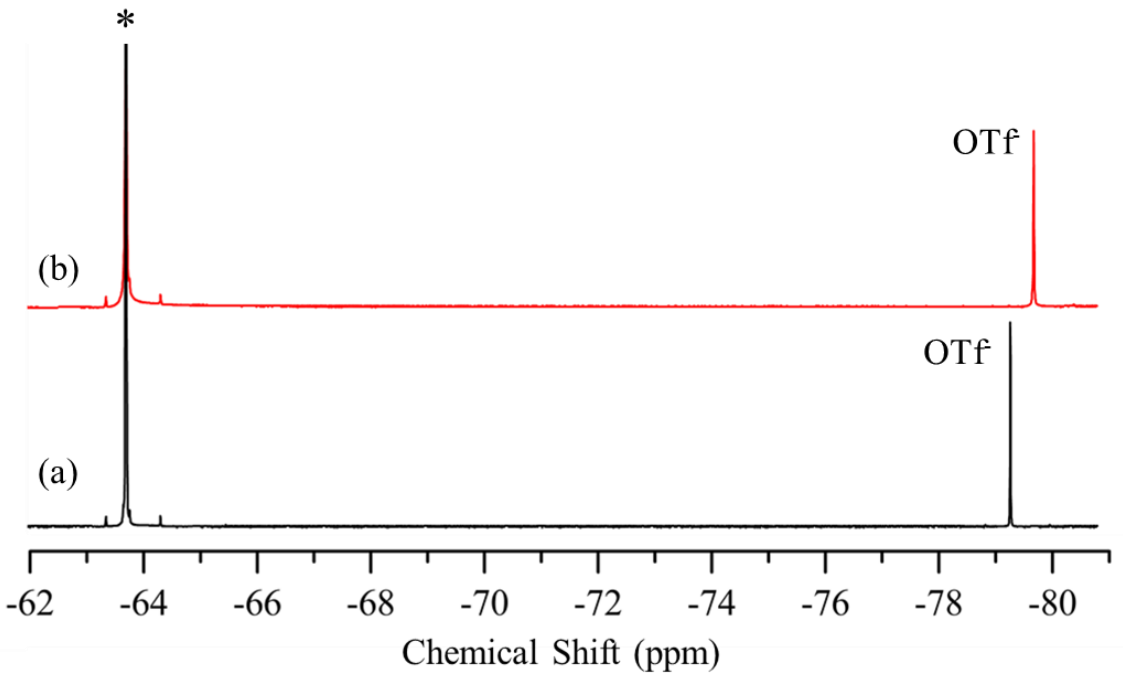

Figure S13. Variable temperature ^{19}F NMR spectra of **3** in CD_3CN at (a) 24 °C and (b) -40 °C. 1,1,1-trifluorotoluene internal standard designated with an asterisk (*).

The OTf^- peak in the ^{19}F NMR exhibits no broadening as the temperature is cooled, consistent with the OTf^- remaining unbound in solution. Shifting in the peak position of free triflate is commonly seen for high-spin ferrous complexes,[1] and likely results from the effects of temperature on magnetization (Curie's Law).

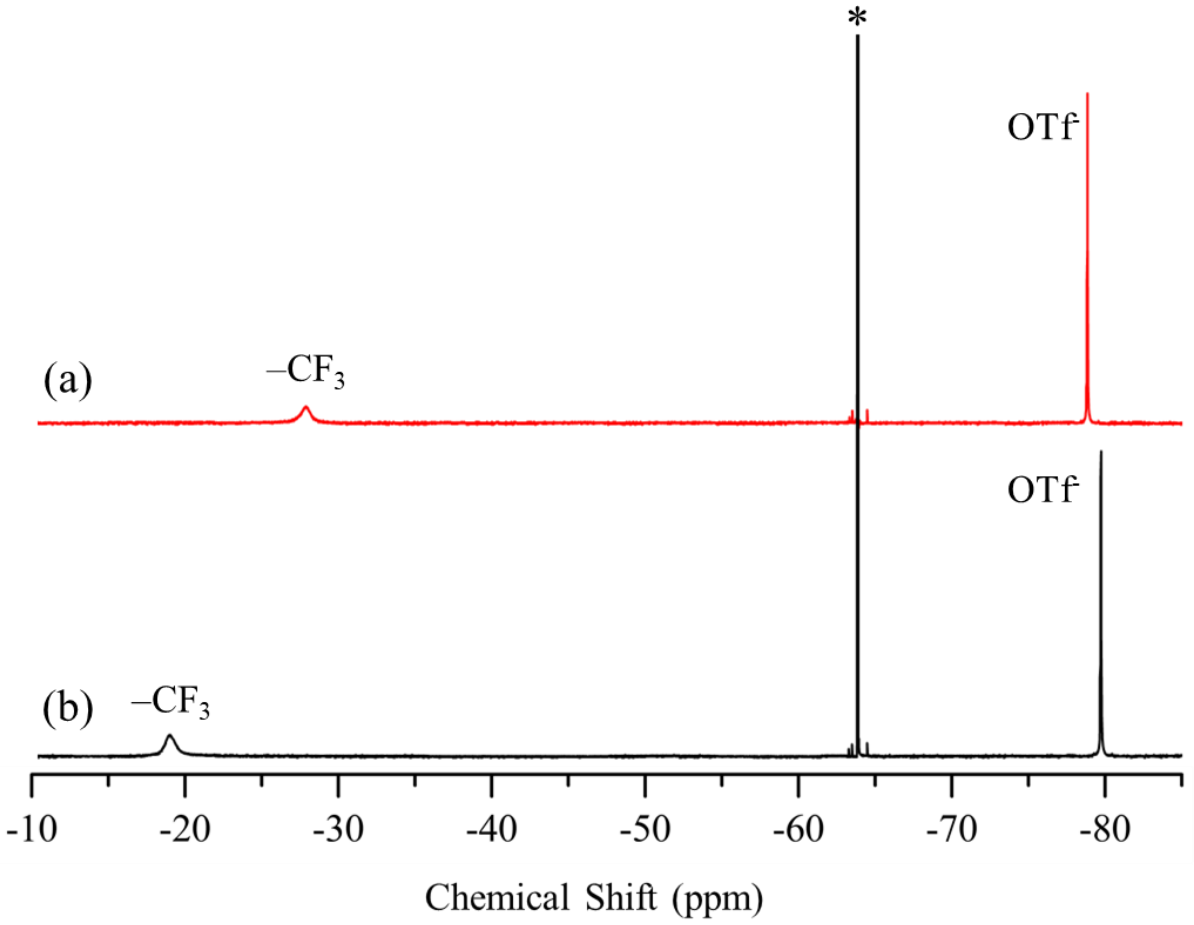

Figure S14. Variable temperature ^{19}F NMR spectra of **4** in CD_3CN at (a) 24 °C and (b) -40 °C. 1,1,1-trifluorotoluene internal standard designated with an asterisk (*).

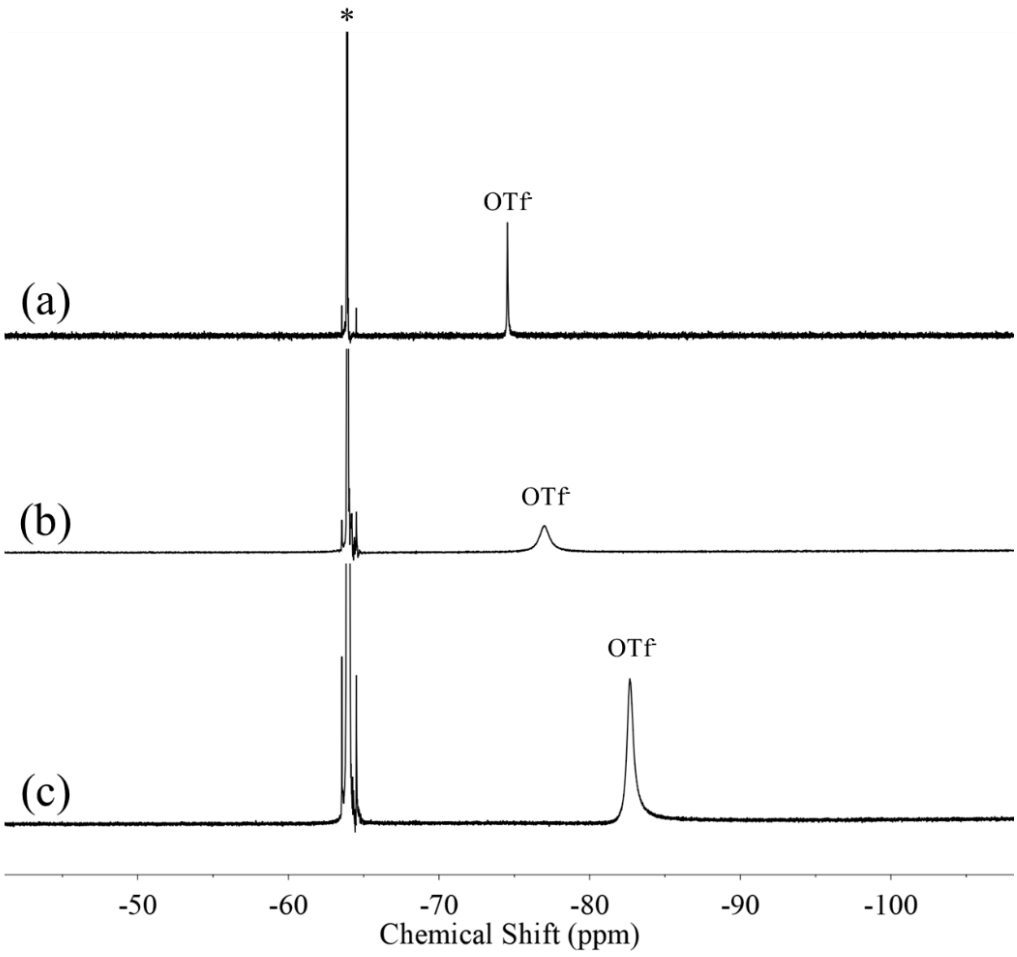

Figure S15. ^{19}F NMR spectrum of **1** in PrCN at (a) 24 °C, (b) -40 °C, and (c) -100 °C. 1,1,1-trifluorotoluene internal standard designated with an asterisk (*).

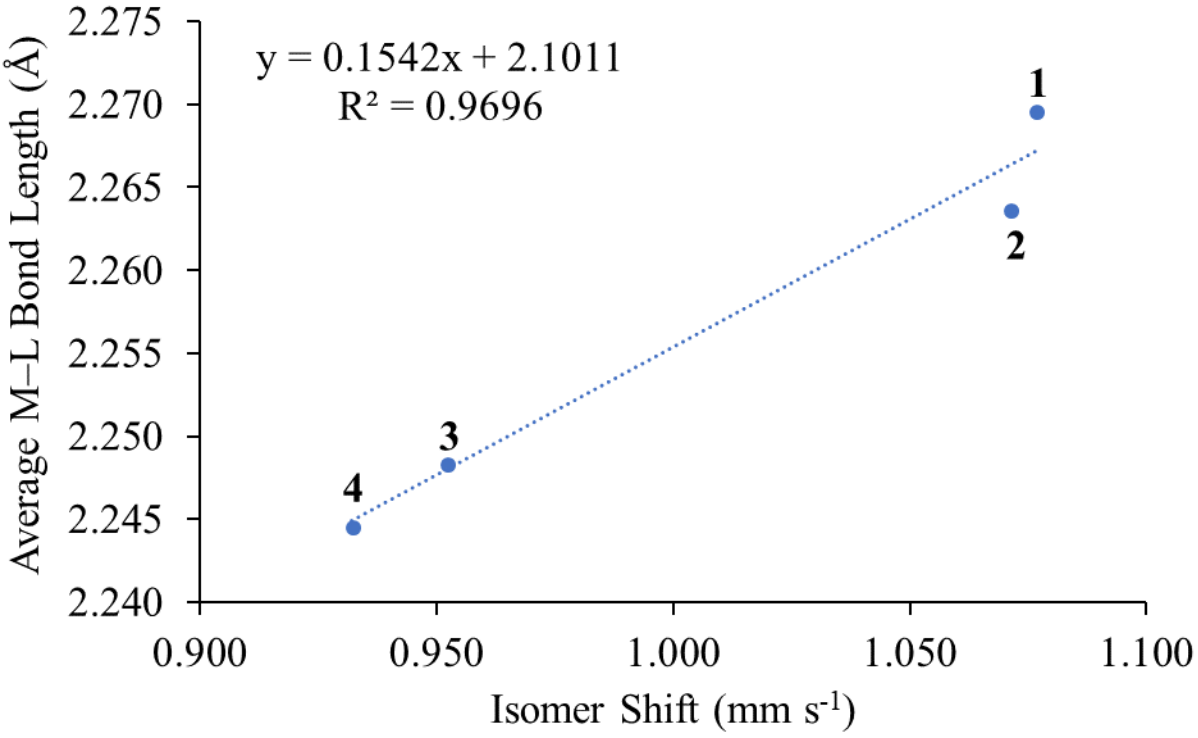

Figure S16. Plot showing correlation between isomer shift and average bond length for all metal–ligand bonds in **1** – **4**.

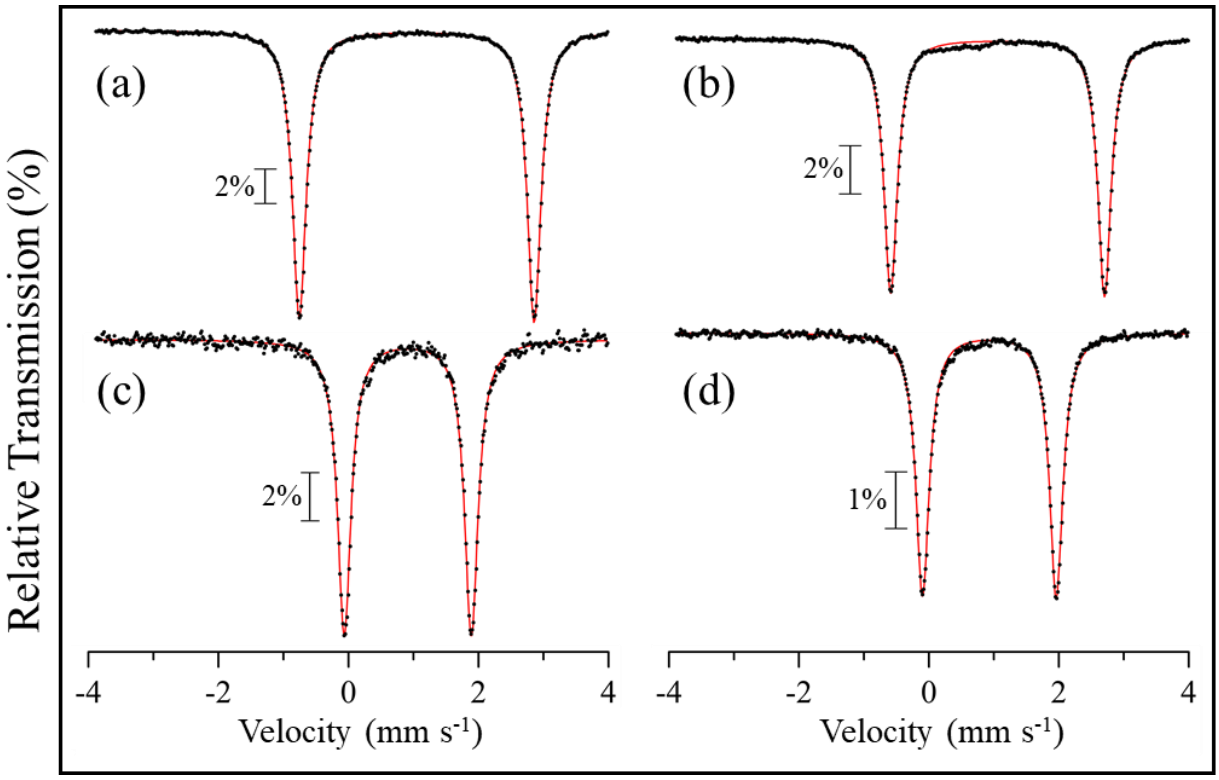

Figure S17. Zero-field ^{57}Fe Mössbauer spectra for (a) **1**, (b) **2**, (c) **3**, and (d) **4** as crystalline solids dispersed in BN matrix at 80 K. Fits shown in red. **1**: $\delta = 1.06$ mm s^{-1}, $|\Delta E_Q| = 3.63$ mm s^{-1}; **2**: $\delta = 1.06$ mm s^{-1}, $|\Delta E_Q| = 3.30$ mm s^{-1}; **3**: $\delta = 0.92$ mm s^{-1}, $|\Delta E_Q| = 1.96$ mm s^{-1}; **4**: $\delta = 0.94$ mm s^{-1}, $|\Delta E_Q| = 2.06$ mm s^{-1}.

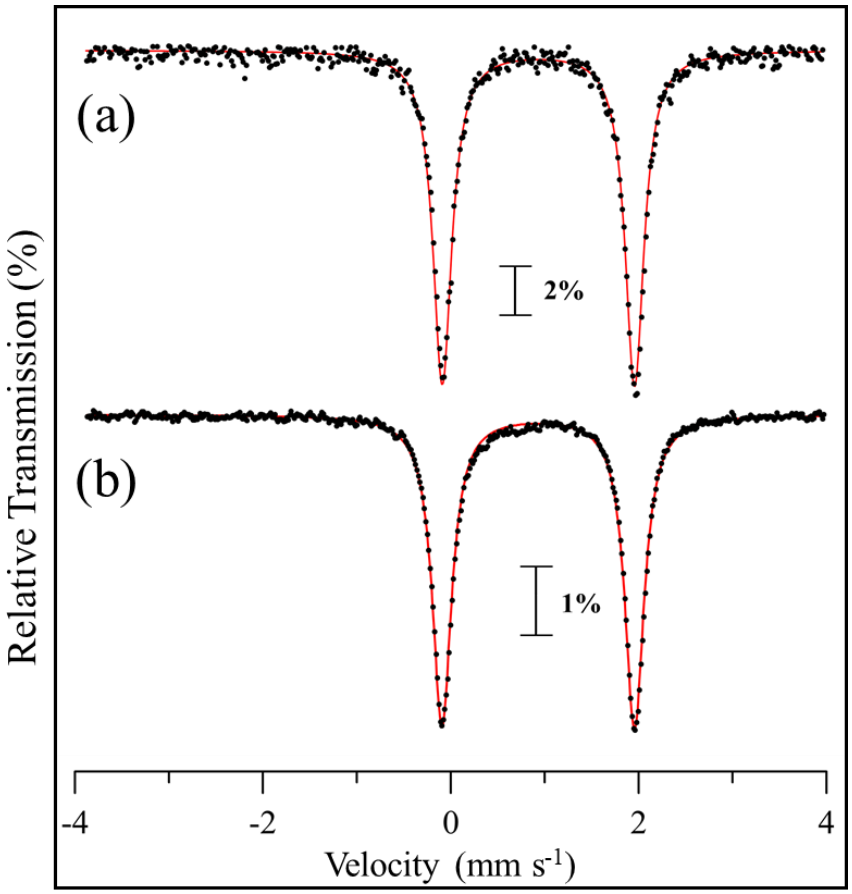

Figure S18. Zero-field ^{57}Fe Mössbauer spectra of (a) **4–^{57}Fe** dissolved in CH_3CN and (b) **4** as a crystalline solid dispersed in BN matrix at 80 K. Fits shown in red. Solid: δ = 0.94 mm s^{-1}, $|\Delta E_Q|$ = 2.06 mm s^{-1}. Solution: δ = 0.95 mm s^{-1}, $|\Delta E_Q|$ = 2.06 mm s^{-1}.

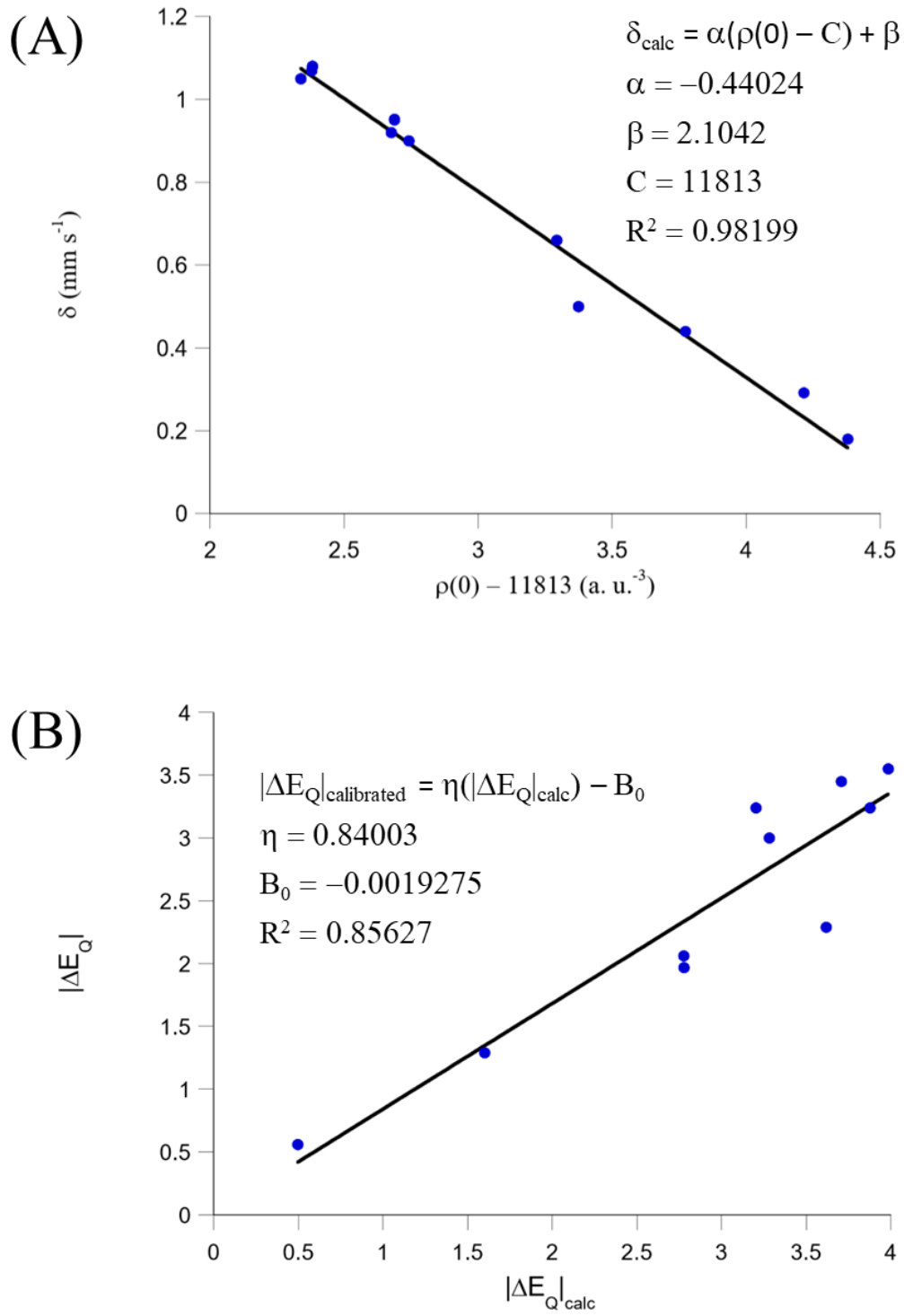

Figure S19. (A) Plot of experimental δ versus ρ(0) – 11813 to calibrate DFT-calculated isomer shifts. (B) Plot of experimental $|\Delta E_Q|$ versus calculated $|\Delta E_Q|$ to calibrate DFT-calculated quadrupole splitting values. Data (Table S7) are plotted as solid blue circles, with the least squares linear regression plotted as a solid black line.

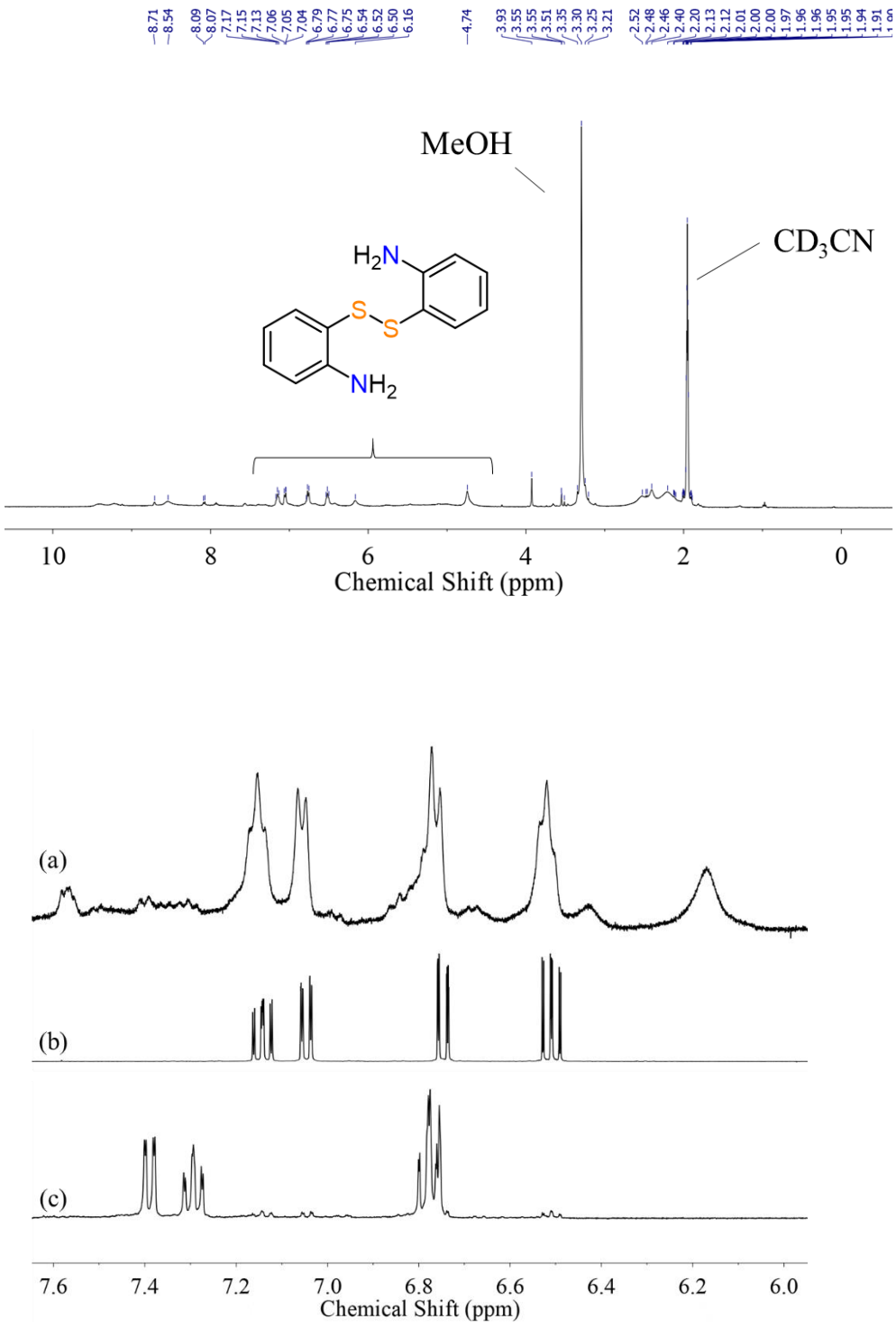

Figure S20. ^{1}H NMR spectrum of reaction of **1** with O_2 at 23 °C in CD_3CN (top). ^{1}H NMR spectra in CD_3CN (aromatic region) of (a) reaction of **1** with O_2 at 23 °C, (b) pure 2-aminophenyl disulfide, and (c) methyl 2-aminobenzenesulfinate from reaction of **1** with O_2 at -95 °C.

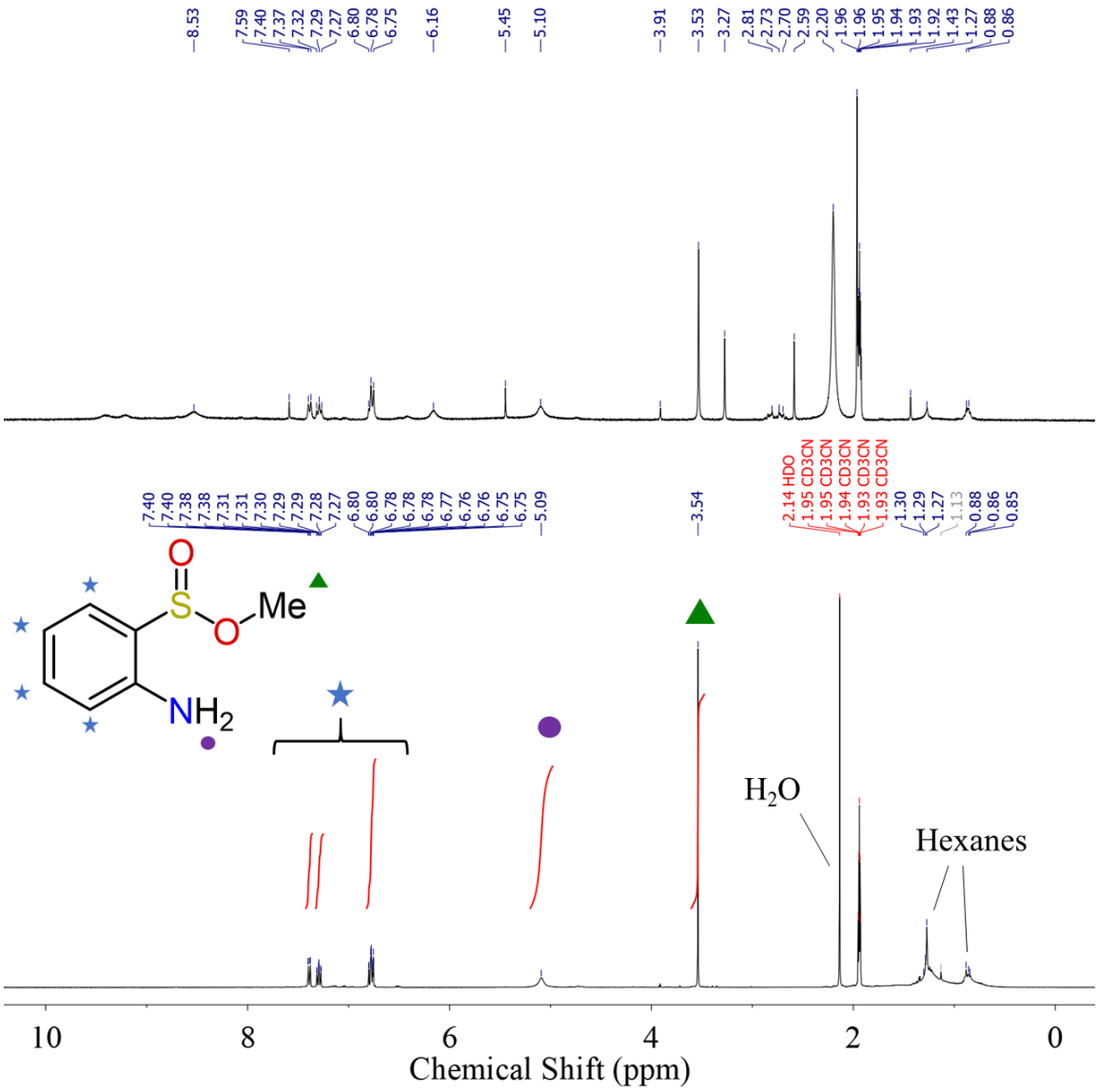

Figure S21. ^{1}H NMR in CD_3CN of (a) crude and (b) purified reaction product from oxygenation of **1** in MeOH at -95 °C.

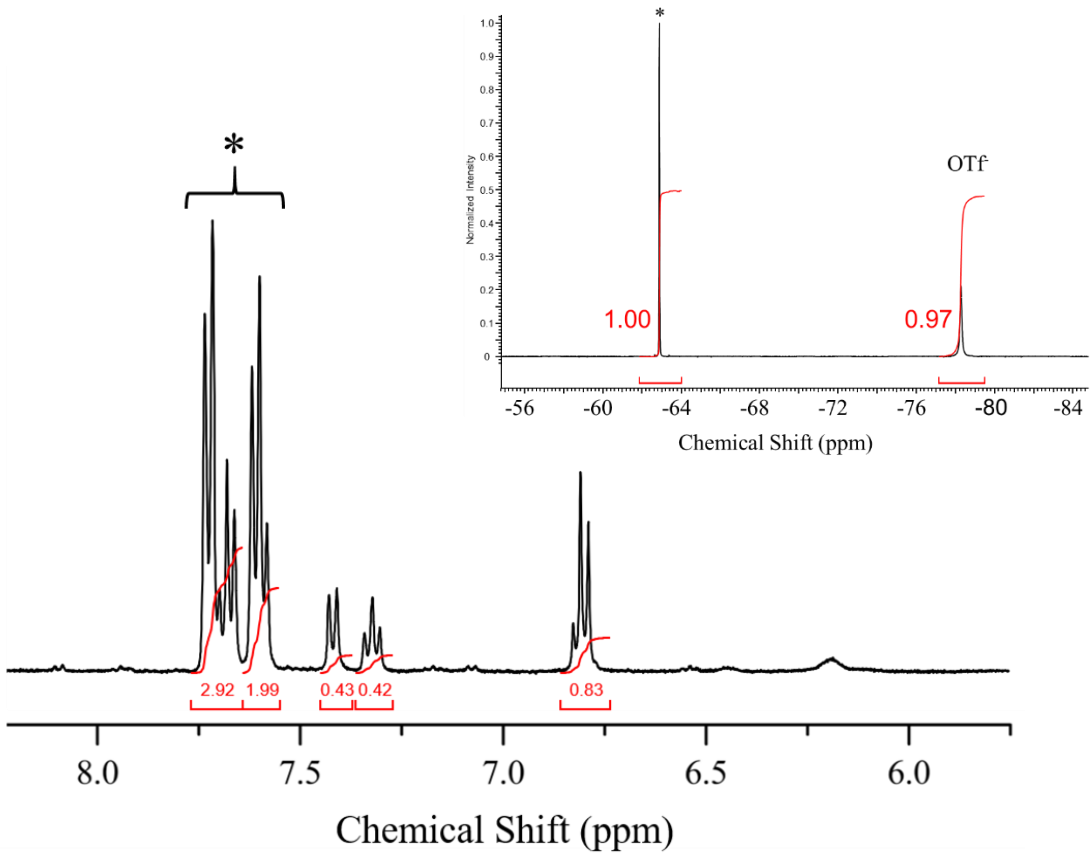

Figure S22. Quantification of 2-amino methyl 2-aminobenzenesulfinate. ^{1}H NMR spectra of reaction of **1** with O_2 at -95 °C collected in CD_3CN. 1,1,1-trifluorotoluene internal standard in designated with an asterisk (*). 1,1,1-trifluorotoluene internal standard designated with an asterisk (*). Inset: ^{19}F NMR of crude reaction mixture in CD_3CN showing 1:1 stoichiometry between complex and internal standard.

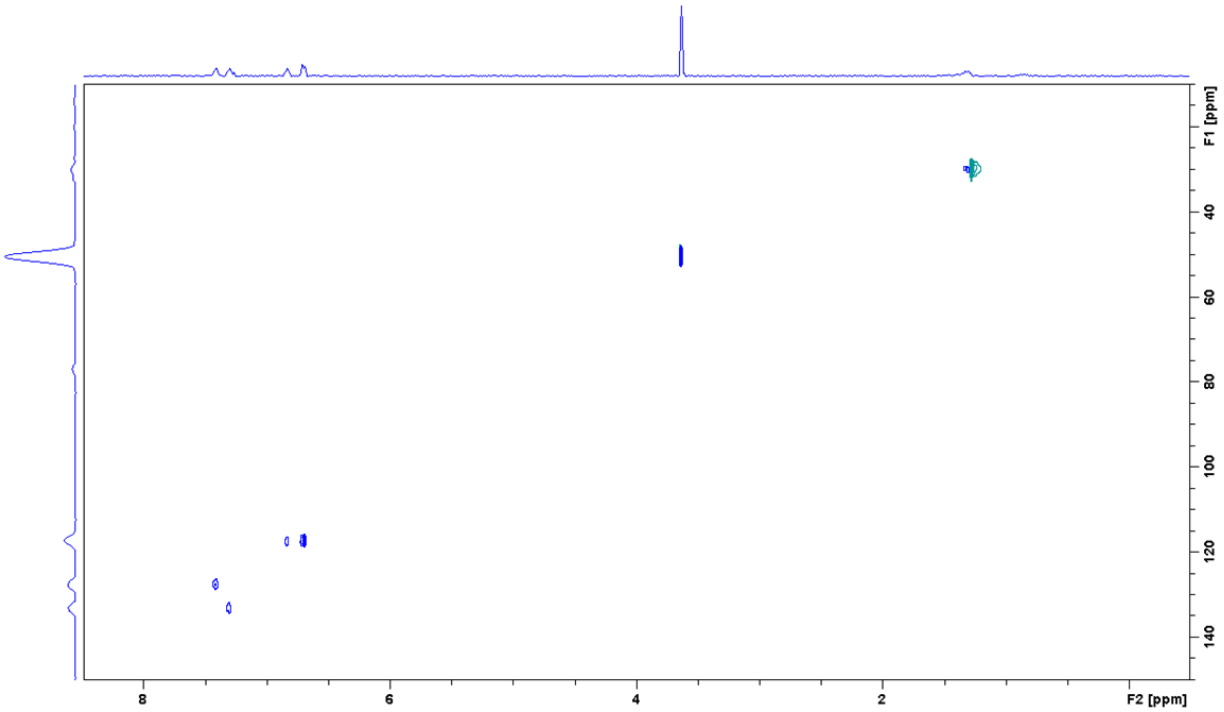

Figure S23. Two-dimensional $^{1}H–^{13}C$ HSQC spectrum of methyl 2-aminobenzenesulfinate from reaction of **1** with O_2 at -95 °C in $CDCl_3$.

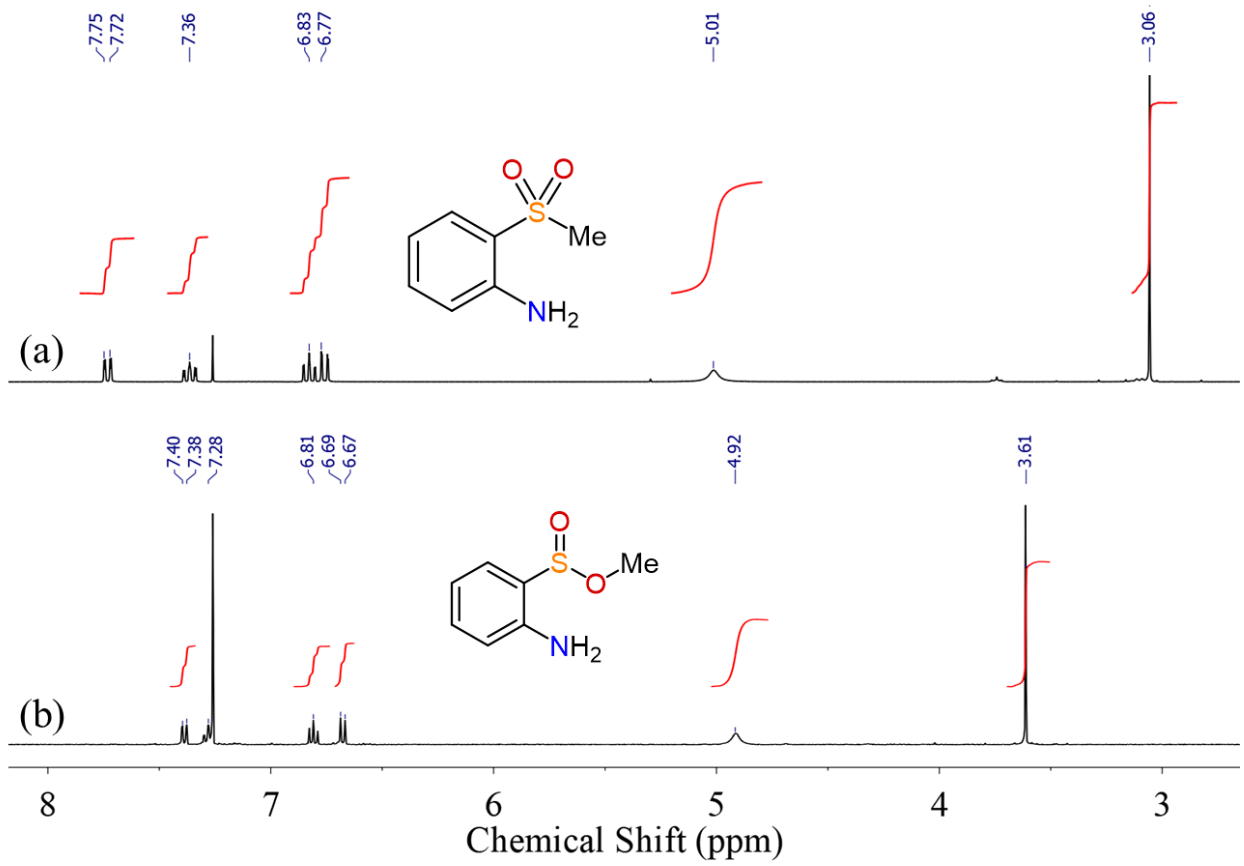

Figure S24. ^{1}H NMR spectra in $CDCl_3$ of (a) 2-methylsulfonylaniline (synthesized independently) and (b) reaction of **1** + excess O_2 at -95 °C. Comparison of (a) and (b), as well as the corresponding ^{13}C NMR spectra (not shown), rule out the sulfone in (a) as the product from the reaction of **1** + excess O_2. The chemical shifts associated with the OMe group in the ^{1}H and ^{13}C NMR spectra of the reaction product ($\delta_{^{1}H}$ = 3.61 ppm ; $\delta_{^{13}C}$ = 50.45 ppm) are shifted compared with those of 2-methylsulfonylaniline ($\delta_{^{1}H}$ = 3.06 ppm ; $\delta_{^{13}C}$ = 42.19 ppm), and fall in the range of other methyl sulfinate esters ($\delta_{^{1}H}$ = 3.47 – 3.80 ppm; $\delta_{^{13}C}$ = 49 – 51 ppm).[2]

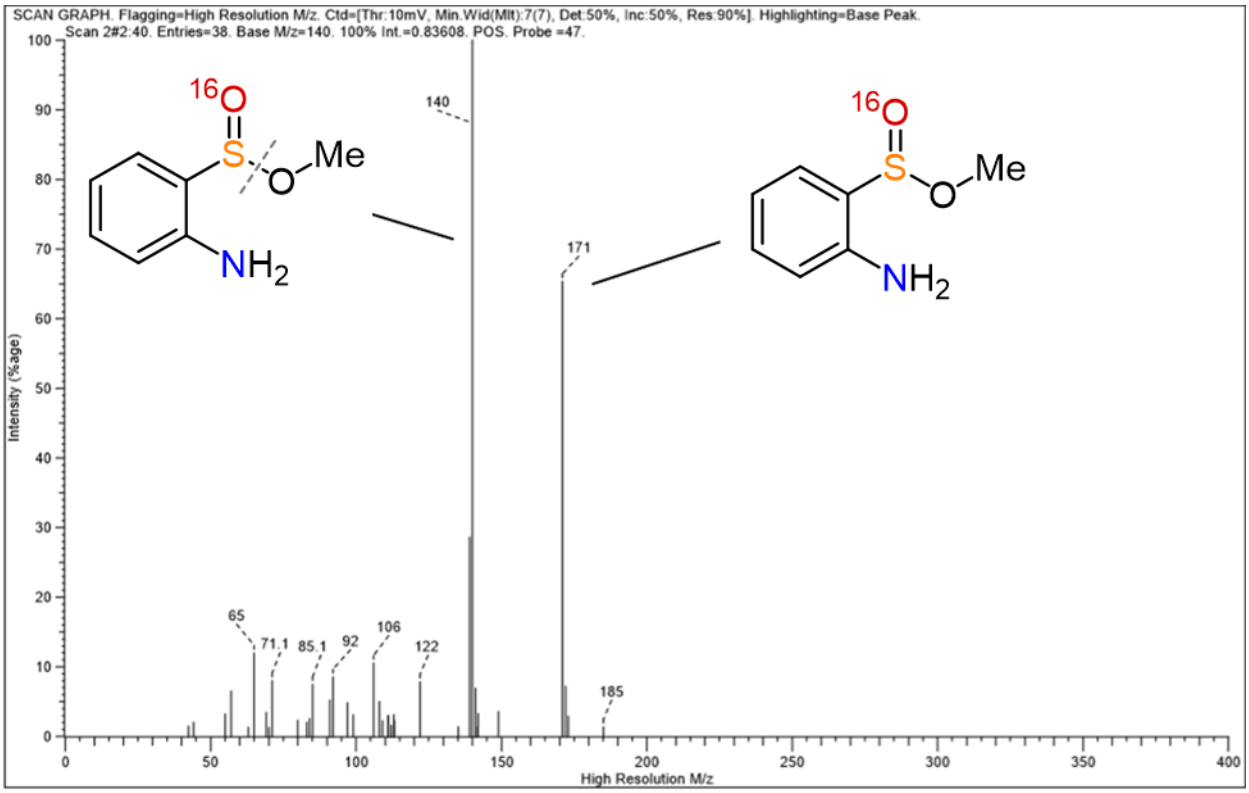

Figure S25. EI-MS spectrum collected in $CHCl_3$ of the product from reaction of **1** + excess O_2 in MeOH at -95 °C.

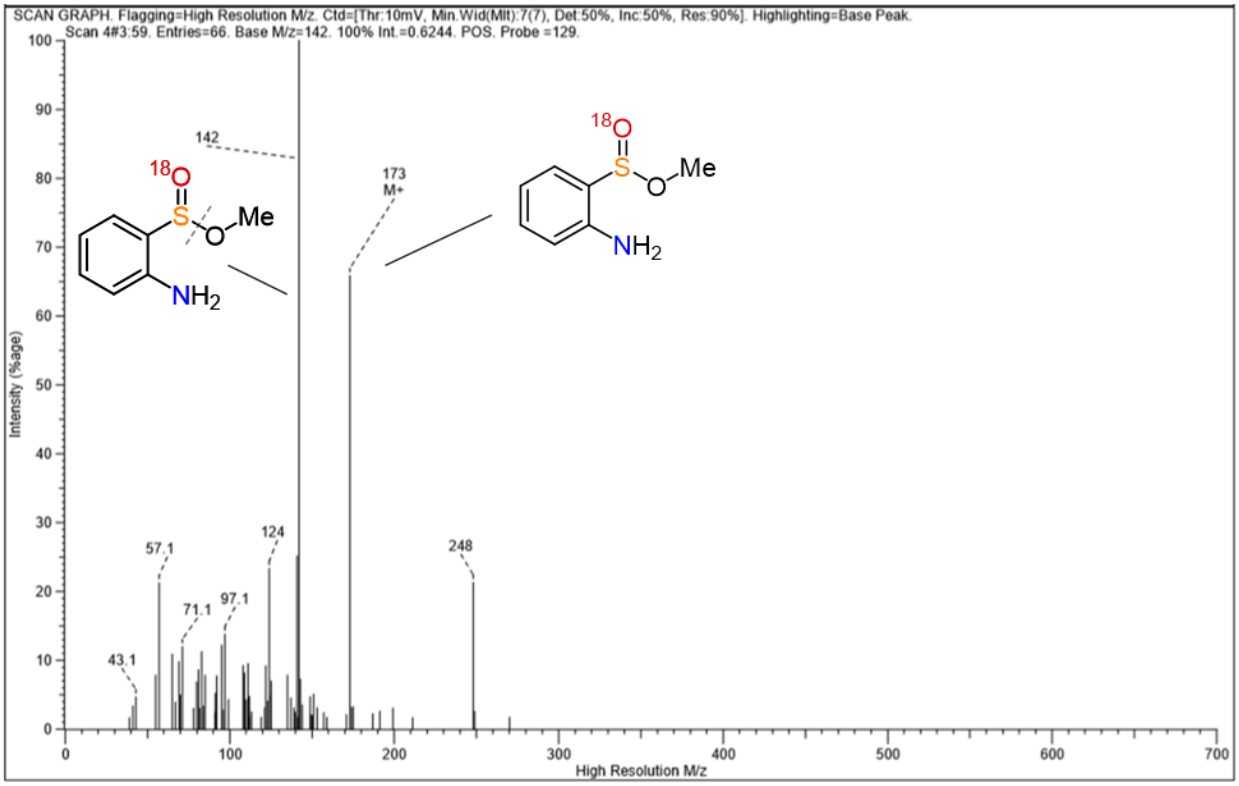

Figure S26. EI-MS spectrum collected in $CHCl_3$ of the product from reaction of **1** + excess $^{18}O_2$ in MeOH at -95 °C.

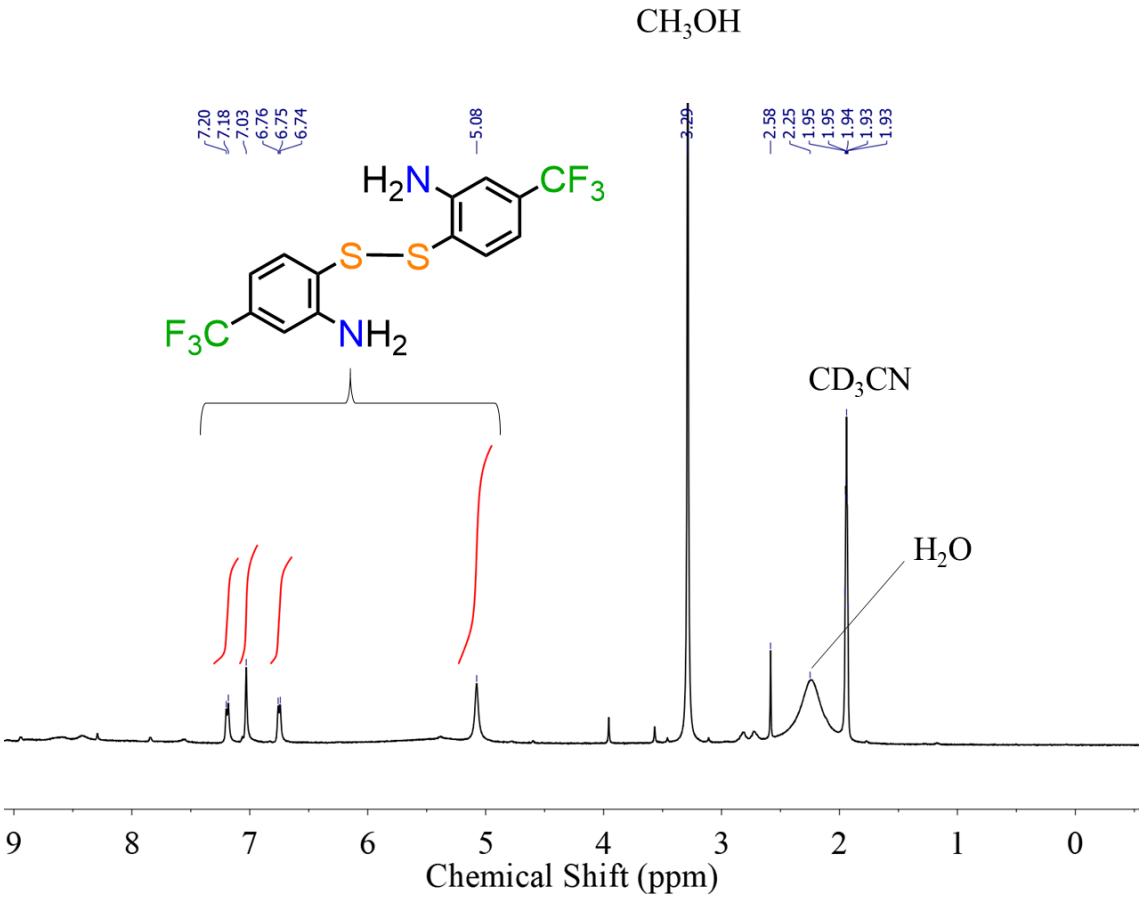

Figure S27. ^{1}H NMR spectra of reaction of **2** + excess O_2 in CD_3CN at 23 °C.

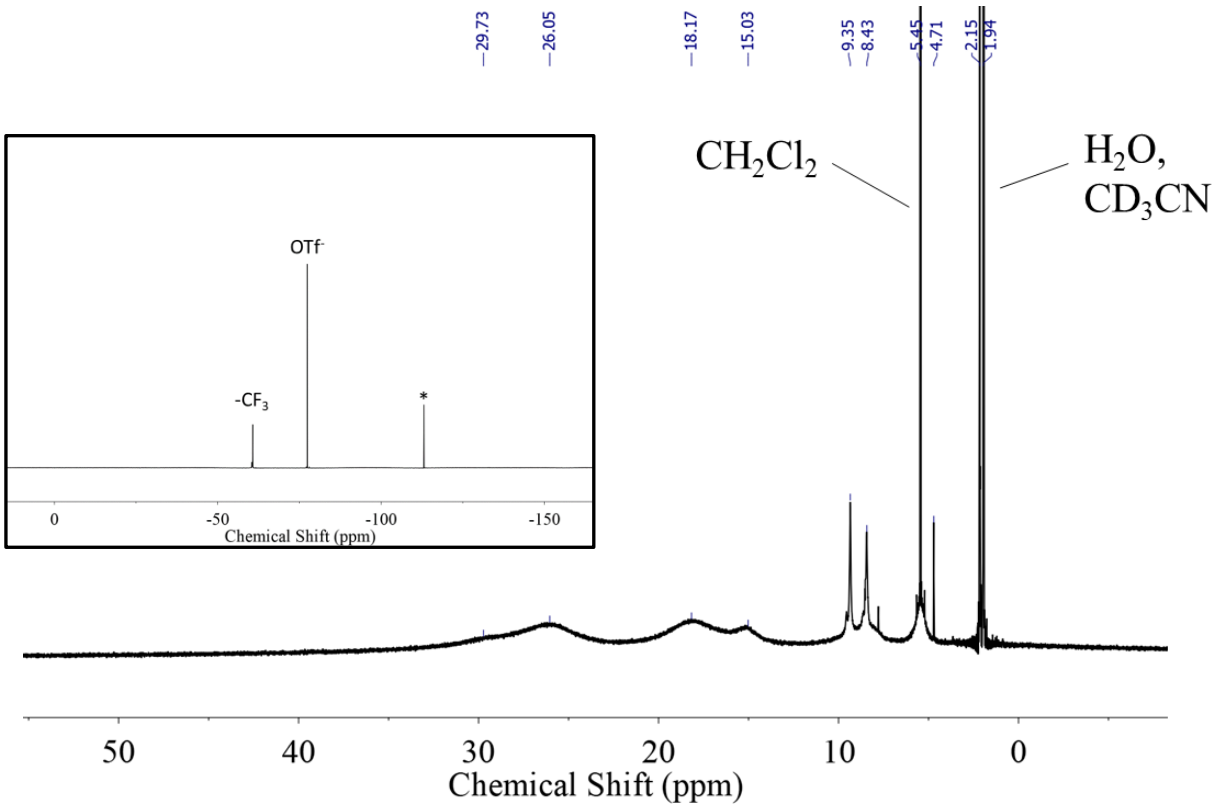

Figure S28. ^{1}H NMR spectrum of crystalline **5** in CD_3CN. Inset: ^{19}F NMR spectrum. Fluorobenzene internal standard designated with an asterisk (*).

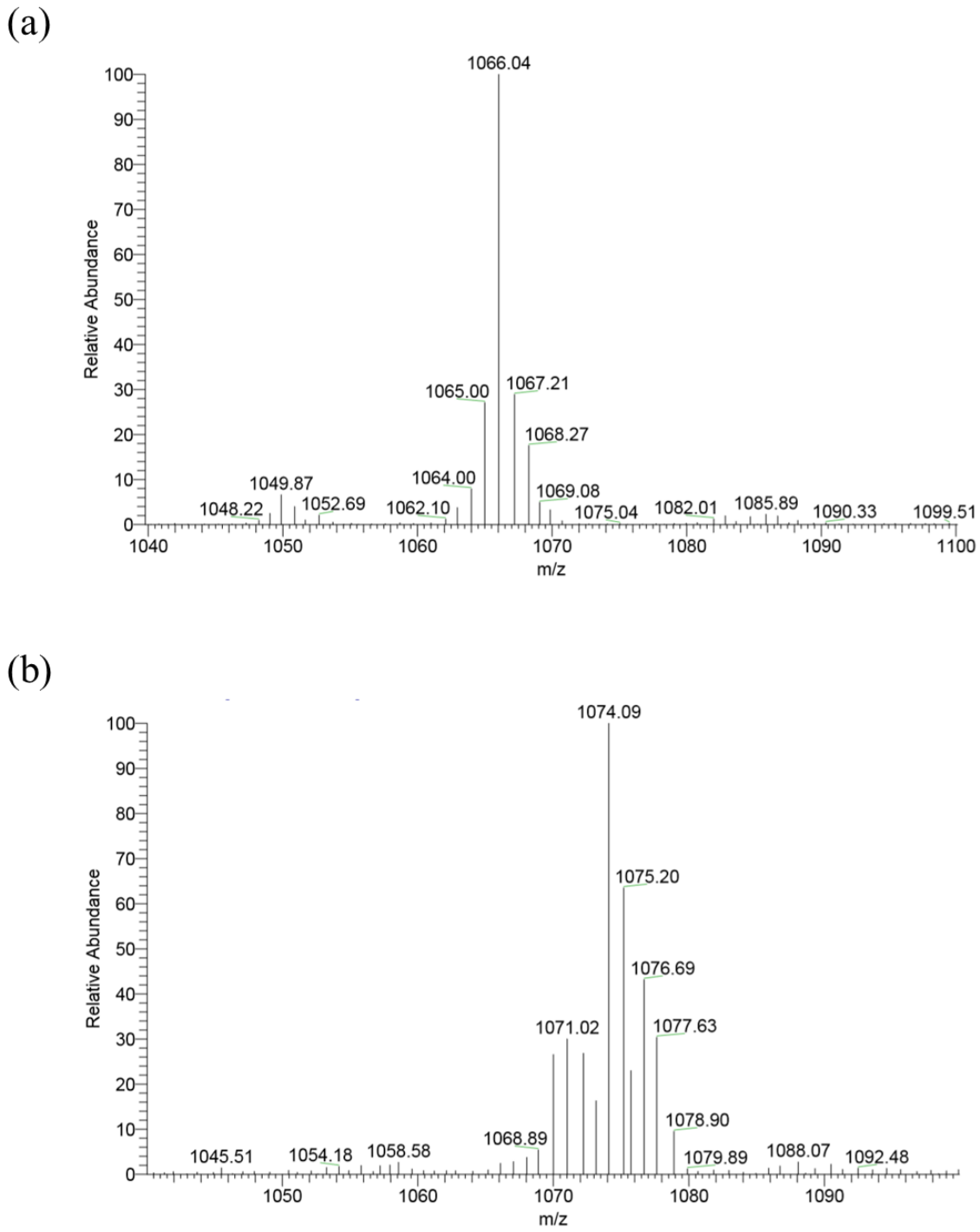

Figure S29. ESI-MS spectra of **5** in CH_3CN generated from (a) $^{16}O_2$ showing m/z consistent with $[(Fe^{III}_2(Me_3TACN)_2(abt)_2)] + 5O – 1H + 1OTf^-$ and (b) $^{18}O_2$ showing an increase in m/z of 8 and 10 units.

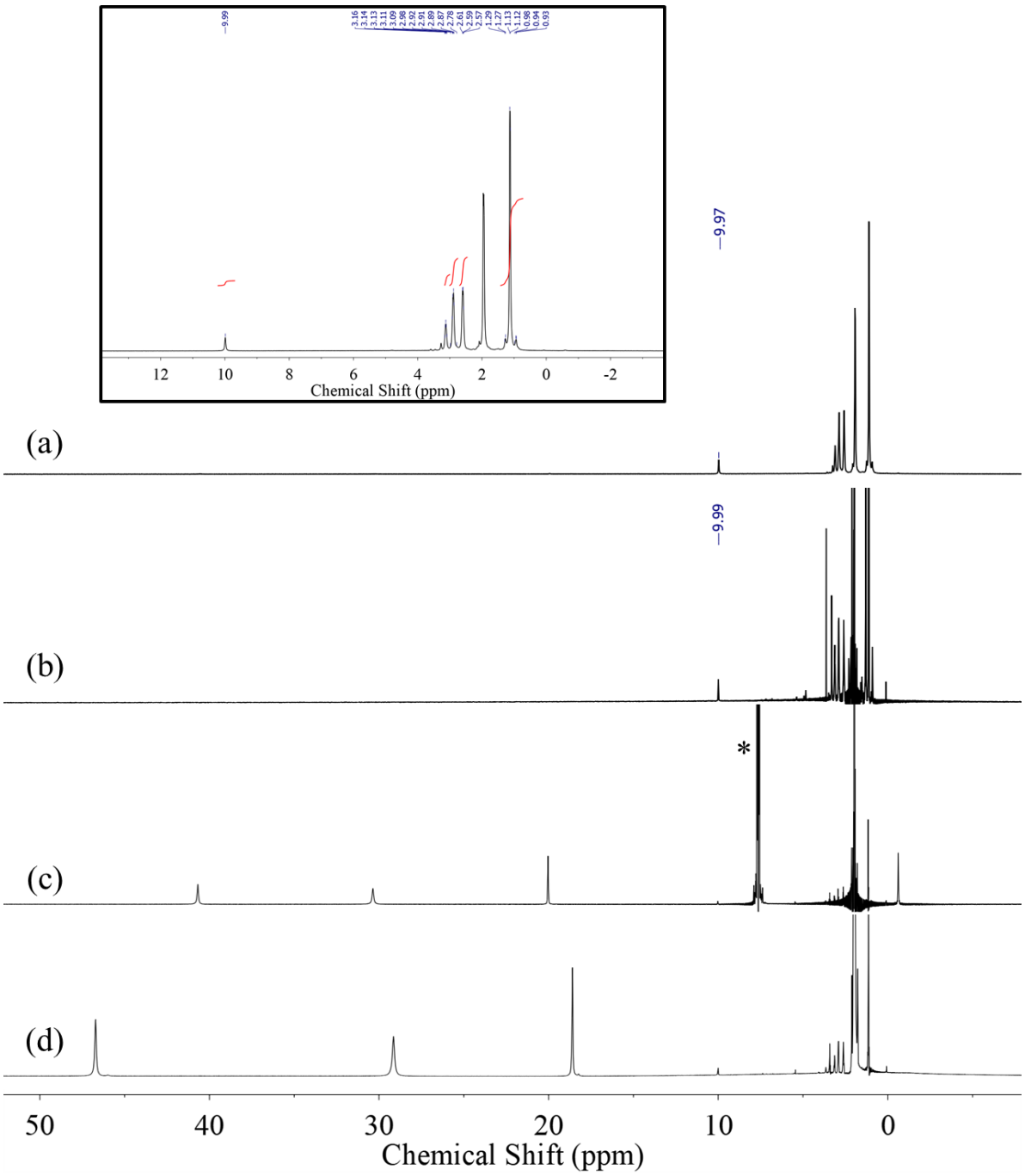

Figure S30. ^{1}H NMR spectra showing decomposition of (a) **3** and (b) **4** to $[iPr_3TACNH]^+$ in MeOH after dissolution in MeOH, solvent removal, and redissolution in CD_3CN. ^{1}H NMR spectra of intact **3** and **4** in CD_3CN shown in (c) and (d), respectively. 1,1,1-trifluorotoluene internal standard designated with an asterisk (*). Inset: Diamagnetic region of spectrum (a).

Single Crystal X-ray Crystallography

All reflection intensities were measured at 110(2) K using a SuperNova diffractometer (equipped with Atlas detector) with either Mo *K*α radiation (λ = 0.71073 Å) for compounds **1**, **2**, **4**, **5** or Cu *K*α radiation (λ = 1.54178 Å) for compound **3** under the program CrysAlisPro (Versions 1.171.36.32 Agilent Technologies, 2013 or 1.171.39.29c, Rigaku OD, 2017). The same program was used to refine the cell dimensions and for data reduction. All structures were solved with the program SHELXS-2014/7[3] or SHELXS-2018/3[3] and were refined on F^2 with SHELXL-2014/7[3] or SHELXL-2018/3.[3] Numerical absorption corrections based on gaussian integration over a multifaceted crystal model or analytical numeric absorption corrections using a multifaceted crystal model were applied using CrysAlisPro. The temperature of the data collection was controlled using the system Cryojet (manufactured by Oxford Instruments). The H atoms were placed at calculated positions (unless otherwise specified) using the instructions AFIX 13 (only for compounds **3** and **4**), AFIX 23, AFIX 43 or AFIX 137 with isotropic displacement parameters having values 1.2 or 1.5 *U*eq of the attached C atoms.

Compound 1: The H atoms attached to N4 were found from difference Fourier maps, and their coordinates were refined freely. The ligand C1→C9 (including N1, N2 and N3) is disordered over two orientations, and the occupancy factor of the major component of the disorder refines to 0.657(5).

Compound 2: The H atoms attached to N4 were found from difference Fourier maps, and their coordinates were refined pseudofreely using the DFIX restraints. The 1,4,7-trimethyl-1,4,7-triazacyclononane ligand is found disordered over two orientations. The occupancy factor of the major component of the disorder refines to 0.507(5).

Compounds 3: The H atoms attached to N4 were found from difference Fourier maps, and their coordinates were refined freely.

Compound 4: The H atoms attached to N4 were found from difference Fourier maps, and their coordinates were refined pseudofreely using the DFIX restraints. The absolute configuration was

established by anomalous-dispersion effects in diffraction measurements on the crystal. The Flack and Hooft parameters both refine to -0.011(4).

Compound 5: The H atoms attached to N4 were found from difference Fourier maps, and their coordinates were refined pseudofreely using the DFIX instruction to keep the N–H distances within acceptable ranges. The Fe complex is located at a site of twofold axial symmetry and only one half of the molecule is crystallographically independent. The $-CF_3$ group and triflate counterion are found to be disordered over two orientations, and the occupancy factors of the major component of the disorder refine to 0.925(5) and 0.785(6), respectively.

Table S1. Experimental details for compound 1

	1
Crystal data	
Chemical formula	$C_{16}H_{27}F_3FeN_4O_3S_2$
M_r	500.38
Crystal system, space group	Monoclinic, $P2_1/n$
Temperature (K)	110
a, b, c (Å)	8.5954 (2), 20.9367 (5), 12.2537 (4)
β (°)	106.051 (3)
V (Å^3)	2119.20 (10)
Z	4
Radiation type	Mo $K\alpha$
μ (mm^{-1})	0.96
Crystal size (mm)	0.46 × 0.18 × 0.16
Data collection	
Diffractometer	SuperNova, Dual, Cu at zero, Atlas diffractometer
Absorption correction	Gaussian *CrysAlis PRO*, Agilent Technologies, Version 1.171.36.32 (release 02-08-2013 CrysAlis171 .NET) (compiled Aug 2 2013,16:46:58) Numerical absorption correction based on gaussian integration over a multifaceted crystal model
T_{min}, T_{max}	0.420, 1.000
No. of measured, independent and observed [$I > 2\sigma(I)$] reflections	29614, 4854, 4273
R_{int}	0.030
$(\sin\theta/\lambda)_{max}$ (Å^{-1})	0.650
Refinement	
$R[F^2 > 2\sigma(F^2)]$, $wR(F^2)$, S	0.027, 0.065, 1.03
No. of reflections	4854
No. of parameters	383
No. of restraints	369
H-atom treatment	H atoms treated by a mixture of independent and constrained refinement
$\Delta\rho_{max}$, $\Delta\rho_{min}$ (e Å^{-3})	0.45, -0.30

Table S2. Experimental details for compound 2

	2
Crystal data	
Chemical formula	$C_{17}H_{26}F_6FeN_4O_3S_2$
M_r	568.39
Crystal system, space group	Monoclinic, $P2_1/n$
Temperature (K)	110
a, b, c (Å)	8.3436 (2), 23.1460 (6), 12.0896 (5)
β (°)	94.827 (3)
V (Å^3)	2326.47 (13)
Z	4
Radiation type	Mo $K\alpha$
μ (mm^{-1})	0.90
Crystal size (mm)	0.28 × 0.26 × 0.17
Data collection	
Diffractometer	SuperNova, Dual, Cu at zero, Atlas
Absorption correction	Gaussian *CrysAlis PRO*, Agilent Technologies, Version 1.171.36.32 (release 02-08-2013 CrysAlis171 .NET) (compiled Aug 2 2013,16:46:58) Numerical absorption correction based on gaussian integration over a multifaceted crystal model
T_{min}, T_{max}	0.693, 1.000
No. of measured, independent and observed [$I > 2\sigma(I)$] reflections	17959, 5334, 4763
R_{int}	0.025
$(\sin \theta/\lambda)_{max}$ (Å^{-1})	0.650
Refinement	
$R[F^2 > 2\sigma(F^2)]$, $wR(F^2)$, S	0.026, 0.064, 1.05
No. of reflections	5334
No. of parameters	389
No. of restraints	563
H-atom treatment	H atoms treated by a mixture of independent and constrained refinement
$\Delta\rho_{max}$, $\Delta\rho_{min}$ (e Å^{-3})	0.34, -0.40

Table S3. Experimental details for compound 3

	3
Crystal data	
Chemical formula	$C_{21}H_{39}FeN_4S \cdot CF_3O_3S$
M_r	584.54
Crystal system, space group	Monoclinic, $P2_1/c$
Temperature (K)	110
a, b, c (Å)	8.69605 (10), 27.0715 (3), 11.47003 (12)
β (°)	99.8988 (11)
V (Å^3)	2660.02 (5)
Z	4
Radiation type	Cu $K\alpha$
μ (mm^{-1})	6.47
Crystal size (mm)	0.37 × 0.18 × 0.12
Data collection	
Diffractometer	SuperNova, Dual, Cu at zero, Atlas
Absorption correction	Analytical *CrysAlis PRO*, Agilent Technologies, Version 1.171.36.32 (release 02-08-2013 CrysAlis171 .NET) (compiled Aug 2 2013,16:46:58) Analytical numeric absorption correction using a multifaceted crystal model based on expressions derived by R.C. Clark & J.S. Reid. (Clark, R. C. & Reid, J. S. (1995). Acta Cryst. A51, 887-897)
T_{min}, T_{max}	0.254, 0.551
No. of measured, independent and observed [$I > 2\sigma(I)$] reflections	17607, 5222, 4853
R_{int}	0.025
$(\sin \theta/\lambda)_{max}$ (Å^{-1})	0.616
Refinement	
$R[F^2 > 2\sigma(F^2)]$, $wR(F^2)$, S	0.025, 0.062, 1.02
No. of reflections	5222
No. of parameters	331
H-atom treatment	H atoms treated by a mixture of independent and constrained refinement
$\Delta\rho_{max}$, $\Delta\rho_{min}$ (e Å^{-3})	0.28, -0.29

Table S4. Experimental details for compound 4

	4
Crystal data	
Chemical formula	$C_{22}H_{38}F_3FeN_4S \cdot CF_3O_3S$
M_r	652.54
Crystal system, space group	Orthorhombic, *Pna*2$_1$
Temperature (K)	110
a, *b*, *c* (Å)	10.14479 (18), 15.7700 (3), 18.0637 (3)
V (Å^3)	2889.89 (9)
Z	4
Radiation type	Mo *K*α
μ (mm^{-1})	0.74
Crystal size (mm)	0.60 × 0.38 × 0.37
Data collection	
Diffractometer	SuperNova, Dual, Cu at zero, Atlas
Absorption correction	Gaussian *CrysAlis PRO*, Agilent Technologies, Version 1.171.36.32 (release 02-08-2013 CrysAlis171 .NET) (compiled Aug 2 2013,16:46:58) Numerical absorption correction based on gaussian integration over a multifaceted crystal model
T_{min}, T_{max}	0.342, 1.000
No. of measured, independent and observed [$I > 2\sigma(I)$] reflections	41859, 6634, 6456
R_{int}	0.035
$(\sin \theta/\lambda)_{max}$ (Å^{-1})	0.650
Refinement	
$R[F^2 > 2\sigma(F^2)]$, $wR(F^2)$, *S*	0.023, 0.055, 1.06
No. of reflections	6634
No. of parameters	365
No. of restraints	3
H-atom treatment	H atoms treated by a mixture of independent and constrained refinement
$\Delta\rho_{max}$, $\Delta\rho_{min}$ (e Å^{-3})	0.36, -0.22
Absolute structure	Flack x determined using 3009 quotients [(I+)-(I-)]/[(I+)+(I-)] (Parsons,

	Flack and Wagner, Acta Cryst. B69 (2013) 249-259).
Absolute structure parameter	-0.011 (4)

Table S5. Experimental details for compound 5

	5
Crystal data	
Chemical formula	$C_{38}H_{58}F_{12}Fe_2N_{10}O_{11}S_4$
M_r	1298.88
Crystal system, space group	Orthorhombic, *Pbcn*
Temperature (K)	110
a, *b*, *c* (Å)	16.8056 (3), 12.9548 (2), 25.2410 (5)
V (Å^3)	5495.30 (17)
Z	4
Radiation type	Mo *K*α
μ (mm^{-1})	0.783
Crystal size (mm)	0.36 × 0.30 × 0.25
Data collection	
Diffractometer	SuperNova, Dual, Cu at zero, Atlas
Absorption correction	Gaussian *CrysAlis PRO* 1.171.39.29c (Rigaku Oxford Diffraction, 2017) Numerical absorption correction based on gaussian integration over a multifaceted crystal model Empirical absorption correction using spherical harmonics, implemented in SCALE3 ABSPACK scaling algorithm.
T_{min}, T_{max}	0.536, 1.000
No. of measured, independent and observed [$I > 2\sigma(I)$] reflections	80374, 6312, 5597
R_{int}	0.037
(sin θ/λ)$_{max}$ (Å^{-1})	0.650
Refinement	
$R[F^2 > 2\sigma(F^2)]$, $wR(F^2)$, *S*	0.030, 0.075, 1.03
No. of reflections	6312
No. of parameters	417
No. of restraints	363
H-atom treatment	H atoms treated by a mixture of independent and constrained refinement
$\Delta\rho_{max}$, $\Delta\rho_{min}$ (e Å^{-3})	0.51, -0.32

Table S6. Comparison of metrical parameters obtained by single crystal X-ray crystallography and DFT calculations for complexes **1 – 4**.

	1		**2**		**3**		**4**	
	Bond Distances (Å)							
	XRD	DFT	XRD	DFT	XRD	DFT	XRD	DFT
Fe1-S1	2.4352(4)	2.406	2.4343(4)	2.412	2.3573(4)	2.387	2.3753(6)	2.377
Fe1-N1	2.225(6)	2.237	2.220(5)	2.288	2.2818(13)	2.185	2.243(2)	2.288
Fe1-N2	2.274(6)	2.274	2.256(5)	2.230	2.1642(12)	2.189	2.1920(18)	2.172
Fe1-N3	2.263(5)	2.277	2.249(5)	2.241	2.1651(12)	2.220	2.1662(19)	2.177
Fe1-N4	2.2344(13)	2.228	2.2393(12)	2.239	2.2555(13)	2.402	2.2656(19)	2.233
Fe1-O1	2.1497(11)	2.206	2.2190(10)	2.200	———	———	———	———
	Bond Angles (°)							
S1-Fe1-N1	101.60(16)	100.19	100.1(3)	100.63	100.82(3)	100.22	100.33(5)	97.85
S1-Fe1-N2	179.59(18)	179.58	179.0(2)	178.25	136.97(3)	145.39	138.78(5)	141.59
S1-Fe1-N3	101.43(15)	100.83	100.1(2)	99.29	138.07(3)	130.17	137.49(5)	131.79
S1-Fe1-N4	79.29(4)	80.01	79.28(3)	79.80	81.30(3)	79.99	80.61(5)	80.93
S1-Fe1-O1	95.91(3)	95.68	95.24(3)	95.46	———	———	———	———
N4-Fe1-N1	178.45(17)	179.77	179.3(3)	79.58	175.10(5)	179.72	176.81(8)	178.76
N4-Fe1-N2	100.34(17)	99.78	101.4(2)	98.46	100.88(5)	98.40	100.67(7)	98.98
N4-Fe1-N3	99.11(17)	100.29	101.0(2)	103.14	92.93(5)	97.80	94.70(7)	98.36
N4-Fe1-O1	89.59(5)	88.63	88.27(4)	88.79	———	———	———	———
N1-Fe1-O1	91.58(17)	91.24	91.5(2)	91.64	———	———	———	———
N2-Fe1-O1	84.26(17)	84.68	84.1(2)	84.24	———	———	———	———
N3-Fe1-O1	161.75(16)	162.84	163.3(3)	162.42	———	———	———	———
N1-Fe1-N2	78.8(2)	80.02	79.2(3)	81.10	80.64(5)	81.32	80.66(7)	82.09
N1-Fe1-N3	79.5(2)	79.79	79.3(3)	76.33	82.53(5)	82.21	82.54(8)	82.30
N2-Fe1-N3	78.4(2)	79.40	80.5(3)	81.30	84.95(5)	84.43	83.71(7)	86.47

Table S7. Experimental and computed Mössbauer parameters used to calibrate the DFT method.

	δ_{exp} mm s^{-1}	$\rho(0)$ a.u.$^{-3}$	$\lvert\Delta E_Q\rvert_{exp}$ mm s^{-1}	$\lvert\Delta E_Q\rvert_{calc}$ mm s^{-1}
1	1.07	11815.37885	3.55	3.98
2	1.08	11815.38135	3.20	3.88
3	0.92	11815.67674	1.97	2.78
4	0.95	11815.68797	2.06	2.78
$[Fe^{II}(TMCS)]PF_6$ [a]	0.90	11815.74194	3.00	3.28
$[Fe^{III}(N3PyO^{Ph2})(OMe)]ClO_4$ [b]	0.50	11816.37474	1.29	1.60
$[Fe^{II}(N3PyO^{Ph2})(MeCN)]ClO_4$ [b]	1.05	11815.33856	2.29	3.62
$[PPh_4]_2[Fe^{II}(SPh)_4]$ [c]	0.66	11816.29401	3.24	3.20
$[Et_4N]_2[Fe^{III}(N_2S_2)(Cl)]$ [d]	0.29	11817.21535	3.45	3.71
Fe^{II}(tsalen)(py)(CO) [e]	0.18	11817.37982	0.56	0.50

[a]Parameters taken from ref. 4. [b]Parameters taken from ref. 5. [c]Parameters taken from ref. 6. [d]Parameters taken from ref. 7. [e]Parameters taken from ref. 8.

Table S8. Comparison of metrical parameters from DFT calculations for **1−OTf**, **1−MeCN**, **1−PrCN**, **1−MeOH**, and **1−5coord**.

	1–OTf	**1–MeCN**	**1–PrCN**	**1–MeOH**	**1–5coord**
	Bond Distances (Å)				
Fe1−S1	2.406	2.455	2.447	2.419	2.369
Fe1–N1	2.237	2.248	2.260	2.232	2.250
Fe1–N2	2.274	2.285	2.288	2.235	2.198
Fe1–N3	2.277	2.283	2.289	2.203	2.174
Fe1–N4	2.228	2.228	2.225	2.203	2.165
Fe1–(O1/N5)	2.206	2.103	2.098	2.340	—

Table S9. Comparison of metrical parameters from DFT calculations for **2−OTf**, **2−MeCN**, **2−PrCN**, **2−MeOH**, and **2−5coord**.

	2–OTf	**2–MeCN**	**2–PrCN**	**2–MeOH**	**2–5coord**
	Bond Distances (Å)				
Fe1−S1	2.412	2.470	2.461	2.429	2.387
Fe1–N1	2.288	2.293	2.298	2.284	2.282
Fe1–N2	2.230	2.238	2.243	2.194	2.159
Fe1–N3	2.241	2.266	2.270	2.190	2.155
Fe1–N4	2.239	2.239	2.232	2.214	2.173
Fe1–(O1/N5)	2.200	2.100	2.097	2.317	—

Table S10. DFT Calculated Mössbauer parameters for **1−OTf**, **1−MeCN**, **1−PrCN**, **1−MeOH**, **1−5coord, 2−OTf**, **2−MeCN**, **2−PrCN**, **2−MeOH**, and **2−5coord**. [a,b,c]

Complex	δ	$\|\Delta E_Q\|$
1–OTf	1.06	3.35
1–MeCN	1.06	2.48
1–PrCN	1.05	2.96
1–MeOH	1.01	3.48
1–5coord	0.86	2.59
2–OTf	1.06	3.26
2–MeCN	1.06	2.91
2–PrCN	1.05	2.89
2–MeOH	1.02	3.35
2–5coord	0.86	2.47

[a]Isomer shifts were calculated according $\delta_{calc} = \alpha(\rho(0) - C) + \beta$, with $\alpha = -0.44024$ mm s^{-1} a.u.^{3}, $\beta = 2.1042$ mm s^{-1}, and C = 11813 a.u.^{3}. [b]Quadrupole splittings were calibrated according to $|\Delta E_Q|_{calibrated} = \eta(|\Delta E|_{calc}) - B_0$, with η = 0.84003, B_0 = -0.0019275 mm s^{-1}. [c]All values in mm s^{-1}.

Enzymology

C93G CDO was chosen as a model enzyme system to investigate abt binding and reactivity. It was picked because of its comparable reactivity to wild-type CDO, depending on the pH, but its inability to form a crosslink means it is present as only one species simplifying kinetic and binding studies. C93G CDO was purified as previously described.[9]

^{1}H NMR

^{1}H NMR was used to investigate product distribution. Spectra can alter radically in aqueous solvent and also change as a function of pH. Thus, spectra of abt and abt disulfide were measured under the conditions used for enzymatic assays to serve as control spectra.

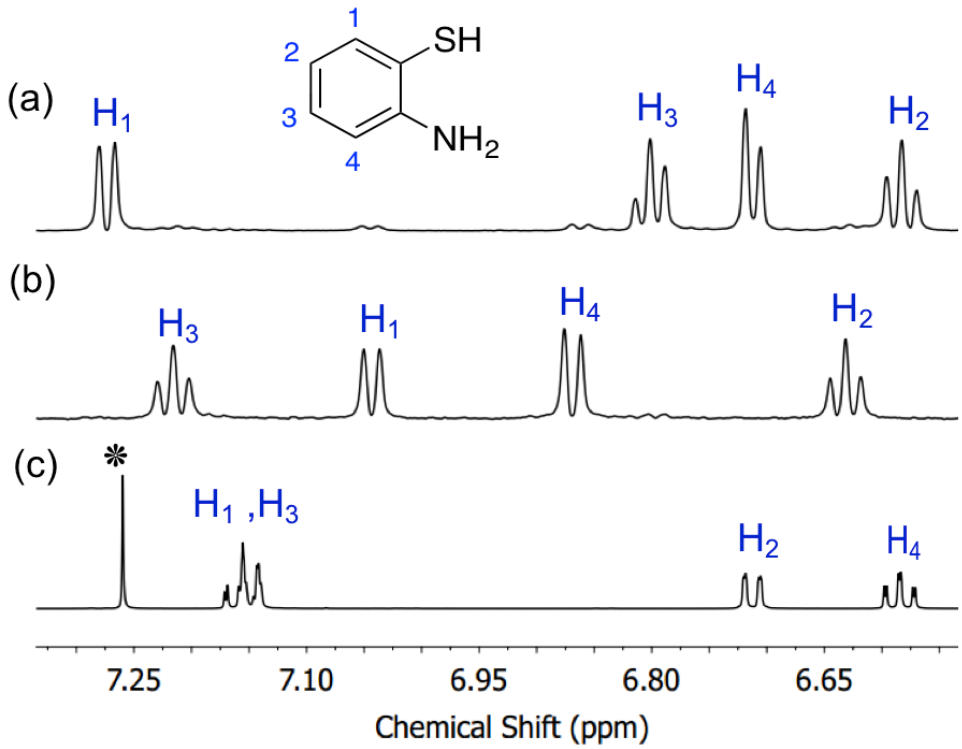

Figure S31. ^{1}H NMR spectra of (a) abt and (b) abt with 2 equiv. H_2O_2 in MOPS buffer pH 7.1 measured in H_2O with a D_2O capillary. (c) Sample b redissolved in $CDCl_3$. (* = $CHCl_3$).

H-ESI Mass spectrometry

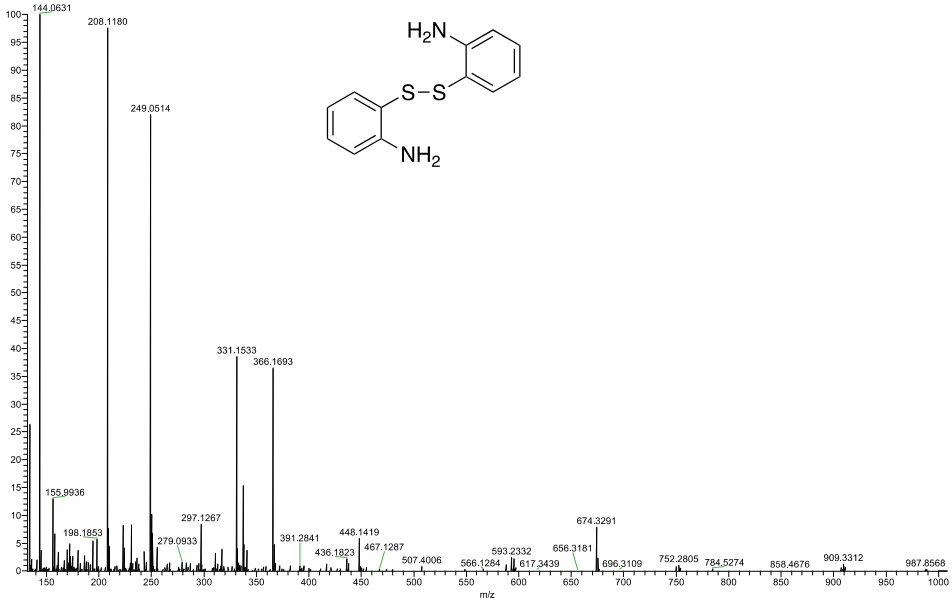

Figure S32. MS spectrum (positive ionization mode) of reaction mixture extracted into acetonitrile of reaction between 10 µM C93G CDO and 5mM abt in Tris buffer pH 8.1.

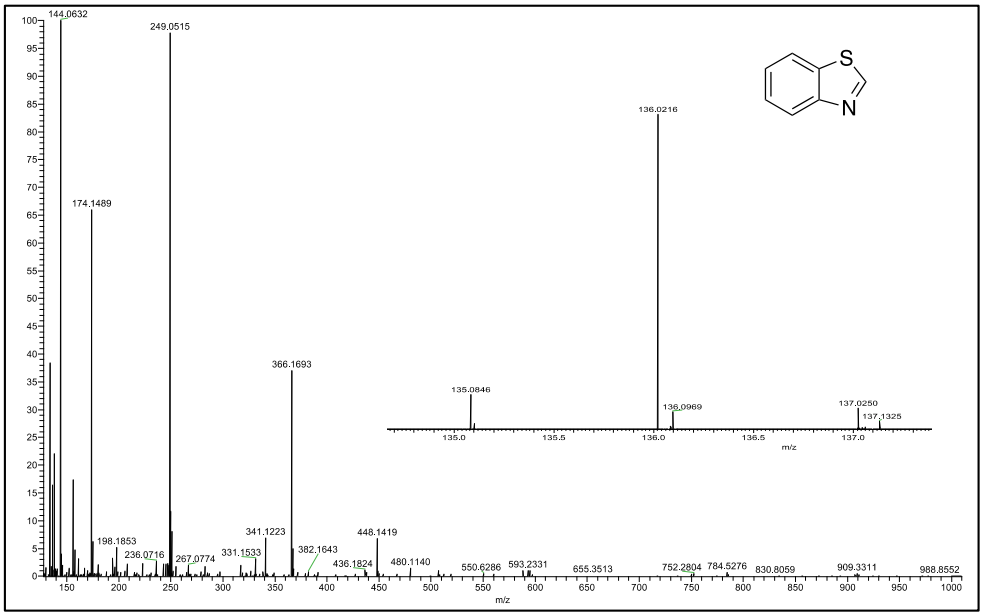

Figure S33. MS spectrum (positive ionization mode) of reaction mixture extracted into acetonitrile of reaction between 10 µM C93G CDO and 5mM abt in Tris buffer pH 8.1 with 20% (v/v) methanol. Inset: A small amount of benzothiazole is also produced.

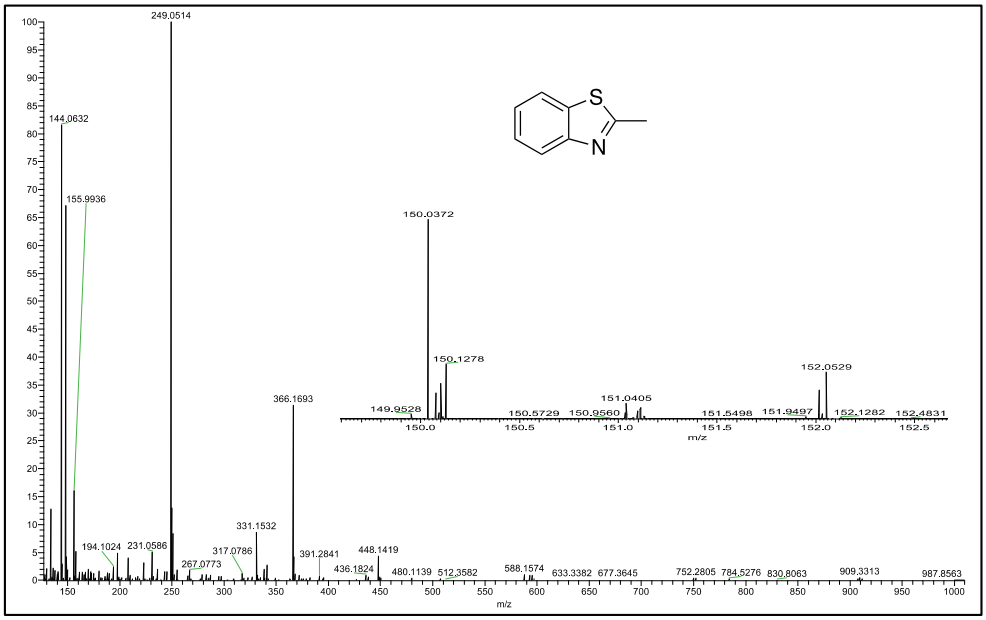

Figure S34. MS spectrum (positive ionization mode) of reaction mixture extracted into acetonitrile of reaction between 10 µM C93G CDO and 5mM abt in Tris buffer pH 8.1 with 20% (v/v) ethanol. Inset: A small amount of 2-methylbenzothiazole is also produced.

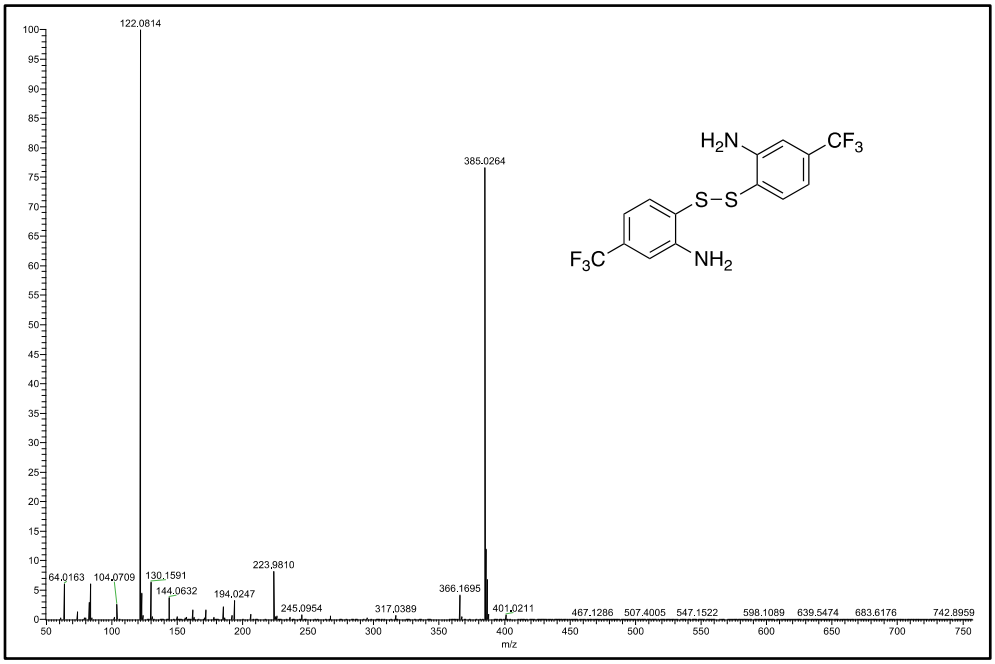

Figure S35. MS spectrum (positive ionization mode) of reaction mixture extracted into acetonitrile of reaction between 10 µM C93G CDO and 5mM abt^{CF3} in Tris buffer pH 7.1.

Extinction coefficients

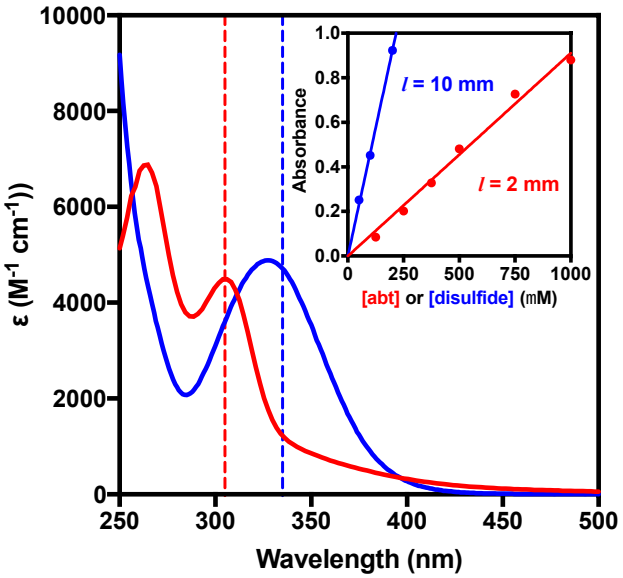

Figure S36. The electronic absorption spectrum of abt (red) and 2-aminophenyl disulfide (blue) in MOPS buffer pH 7.1. Inset: the linear dependence of the absorption with concentration of abt at 305 nm (pathlength = 2 mm) and disulfide at 335 nm (pathlength = 10 mm).

pH profile

The pH dependence of abt oxidation was investigated by measuring reaction velocities at 335 nm at constant enzyme and abt concentration but varying pH. The maximum velocity was found to occur at pH 7.1, which is the pH of maximum activity of C93G CDO with its natural substrate cysteine.[9]

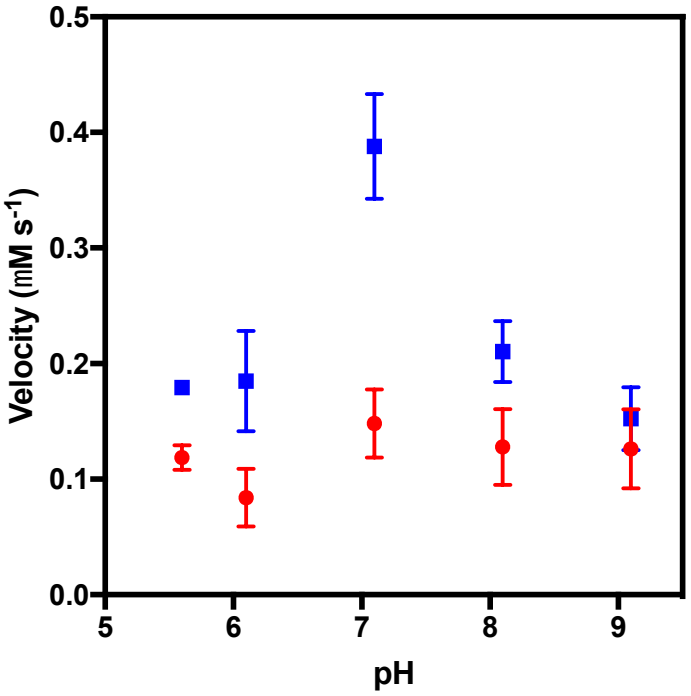

Figure S37. pH profile of abt turnover. The velocities of C93G CDO-mediated (2 μM, blue) and enzyme-free (red) oxidation of 5 mM abt was measured in the following buffers (all 100 mM): MES pH 5.6 and 6.1, MOPS pH 7.1, TRIS pH 8.1 and CHES 9.1, $n \geq 2$, ± SD.

Mössbauer parameters of C93G CDO binding studies with abt

Table S11. ^{57}Fe Mössbauer parameters of C93G CDO in the absence and presence of abt and cysteine measured at 10 K and fitted as a single quadrupole doublet.

Sample	Subspectrum	δ (mm/s)	ΔE_Q (mm/s)	Γ_L (mm/s)	Γ_R (mm/s)
C93G CDO	-	1.25	2.99	0.45	0.48
+ 0.5 eq abt	-	1.24	3.00	0.47	0.50
+ 2.2 eq abt	-	1.20	3.01	0.50	0.50
+ 4.9 eq abt	-	1.23	2.99	0.46	0.52
+ 9.8 eq abt	-	1.21	2.99	0.45	0.51
+ 1 eq cys	A	1.02	2.31	0.49	0.49
	B	1.08	3.05	0.43	0.43

References

(1) Blakesley, D. W.; Payne, S. C.; Hagen, K. S. *Inorg. Chem.* **2000,** *39,* 1979-1989.
(2) Du, B.; Li, Z.; Qian, P.; Han, J.; Pan, Y. *Chem. - Asian J.* **2016,** *11*, 478-481.
(3) Sheldrick, G. M. *Acta Crystallographica. Section C, Structural Chemistry* **2015,** *71,* 3-8.
(4) Bukowski, M. R.; Koehntop, K. D.; Stubna, A.; Bominaar, E. L.; Halfen, J. A.; Münck, E.; Nam, W.; Que, L., Jr. *Science* **2005,** *310,* 1000-1002.
(5) Pangia, T. M.; Davies, C. G.; Prendergast, J. R.; Gordon, J. B.; Siegler, M. A.; Jameson, G. N. L.; Goldberg, D. P. *J. Am. Chem. Soc.* **2018,** *140,* 4191-4194.
(6) Coucouvanis, D.; Swenson, D.; Baenziger, N. C.; Murphy, C.; Holah, D. G.; Sfarnas, N.; Simopoulos, A.; Kostikas, A. *J. Am. Chem. Soc.* **1981,** *103,* 3350-3362.
(7) Chatel, S.; Chauvin, A. S.; Tuchagues, J. P.; Leduc, P.; Bill, E.; Chottard, J. C.; Mansuy, D.; Artaud, I. *Inorg. Chim. Acta* **2002,** *336,* 19-28.
(8) Marini, P. J.; Murray, K. S.; West, B. O. *J. Chem. Soc., Dalton Trans.* **1983**, 143-151.
(9) Davies, C. G.; Fellner, M.; Tchesnokov, E. P.; Wilbanks, S. M.; Jameson, G. N. L. *Biochemistry* **2014,** *53,* 7961-7968.